HHS Public Access

Author manuscript

J Control Release. Author manuscript; available in PMC 2022 September 10.

Published in final edited form as:

J Control Release. 2021 September 10; 337: 179–192. doi:10.1016/j.jconrel.2021.07.018.

Glycosylation of PAMAM Dendrimers Significantly Improves Tumor Macrophage Targeting and Specificity in Glioblastoma

Rishi Sharma[1,§], **Kevin Liaw**[1,2,§], **Anjali Sharma**[1], **Ambar Jimenez**[1], **Michelle Chang**[2], **Sebastian Salazar**[3], **Imaan Amlani**[2], **Sujatha Kannan**[4,5], **Rangaramanujam M Kannan**[1,2,5]

[1]Center for Nanomedicine, Department of Ophthalmology, Wilmer Eye Institute Johns Hopkins University School of Medicine, Baltimore, MD 21231, USA

[2]Department of Chemical and Biomolecular Engineering, Johns Hopkins University, Baltimore MD, 21218, USA

[3]Department of Biomedical Engineering, Johns Hopkins University, Baltimore, MD 21218, USA

[4]Department of Anesthesiology and Critical Care Medicine, Johns Hopkins University School of Medicine, Baltimore, MD 21287, USA

[5]Hugo W. Moser Research Institute at Kennedy Krieger, Inc., Baltimore MD, 21205, USA.

Abstract

Glioblastoma is among the most aggressive forms of cancers, with a median survival of just 15-20 months for patients despite maximum clinical intervention. Majority of conventional anti-cancer therapies fail due to associated off-site toxicities which can be addressed by developing target-specific drug delivery systems. Advances in nanotechnology have provided targeted systems to overcome drug delivery barriers associated with brain and other types of cancers. Dendrimers have emerged as promising vehicles for targeted drug and gene delivery. Dendrimer-mediated targeting strategies can be further enhanced through the addition of targeting ligands to enable receptor-

[§]These authors contributed equally

Conflicts of Interest

The authors have awarded and pending patents relating to the TAMs targeting ability of hydroxyl terminated PAMAM dendrimers. RMK and SK are co-founders and have financial interests in Ashvattha Therapeutics LLC, Orpheris Inc., and RiniSight, three startups involved with the translation of dendrimer drug delivery platforms.

CRediT author statement

Rishi Sharma: Conceptualization, Methodology, Validation, Formal analysis, Investigation, Resources, Data Curation, Writing - Original Draft, Writing - Review & Editing, Visualization

Kevin Liaw: Methodology, Validation, Formal analysis, Investigation, Resources, Data Curation, Writing - Original Draft, Writing - Review & Editing, Visualization

Anjali Sharma: Methodology, Validation, Formal analysis, Investigation, Data Curation, Writing - Original Draft, Writing - Review & Editing, Visualization

Amber Jimenez: Investigation

Michelle Cheng: Investigation

Sebastian Salazer: Investigation

Imaan Almani: Investigation

Sujatha Kannan: Writing - Review & Editing, Project administration, Funding acquisition, Supervision

Rangaramanujam M. Kannan: Writing - Review & Editing, Project administration, Funding acquisition, Supervision

specific interactions. Here, we explore the sugar moieties as ligands conjugated to hydroxyl-terminated polyamidoamine dendrimers to leverage altered metabolism in cancer and immune targeting. Using a highly facile click chemistry approach, we modified the surface of dendrimers with glucose, mannose, or galactose moieties in a well-defined manner, to target upregulated sugar transporters in the context of glioblastoma. We show that glucose modification significantly enhanced targeting of tumor-associated macrophages (TAMs) and microglia by increasing brain penetration and cellular internalization, while galactose modification shifts targeting away from TAMs towards galectins on glioblastoma tumor cells. Mannose modification did not alter TAMs and microglia targeting of these dendrimers, but did alter their kinetics of accumulation within the GBM tumor. The whole body biodistribution was largely similar between the systems. These results demonstrate that dendrimers are versatile delivery vehicles that can be modified to tailor their targeting for the treatment of glioblastoma and other cancers.

Graphical Abstract

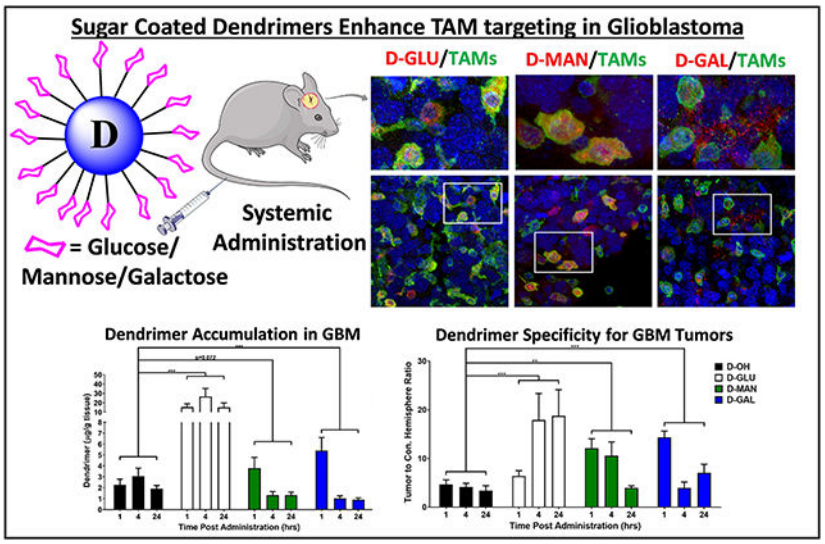

Keywords

Dendrimer; glioblastoma; tumor-associated macrophages; glycosylation; tumor-targeting

Introduction

Glioblastoma is the most common and aggressive form of primary brain cancer, with a median survival time of 16-20 months and 5 year survival rates of less than 5%.[1, 2] It accounts for 70% of brain cancer cases, with more than 14,000 new cases diagnosed in the United States each year.[3] In addition to these poor prognoses, glioblastoma also exerts significant impacts on the quality of life and cognitive functions of patients.[4, 5] Current standard of care consists maximum safe surgical resection followed by intensive chemotherapy and radiotherapy,[6] but this intervention strategy has failed to significantly improve patient outcomes. Therefore, innovative strategies to enhance drug delivery to glioblastoma are necessary to achieve robust improvements to patient outcomes.

In order for systemic therapies for glioblastoma to be effective, they must penetrate the blood brain tumor barrier. In addition, they must then access and accumulate within the cells of interest to achieve relevant therapeutic doses.[7] Tumor-associated macrophages (TAMs) have emerged as promising cellular targets to enable effective tumor therapy due to their roles in regulating the tumor immune response.[8, 9] Tumors secrete immune polarizing signals that recruit host macrophage and resident microglia and repolarize them into TAMs, which suppress tumor-killing immune activation and promote tumor growth, invasion, and drug resistance.[10-12] Therefore, by targeting these TAMs with immunotherapies, we can reprogram the tumor immune response away from the tumor-supporting state and towards the anti-tumor phenotype. Based on strong preclinical results, TAMs-targeted immunotherapies are undergoing clinical trials as single therapies or in combination with traditional treatments in many types of cancers, including glioblastoma (NCT02829723, NCT02452424, NCT01349049, NCT01217229). However, their translation has been limited by low response rates, drug resistance, and off-target immune activation leading to systemic toxicities.[13, 14] Nanotechnology-mediated immunotherapies that specifically target TAMs can provide significant innovation for improved therapeutic efficacy and limited systemic toxicities.

Peptide and small molecule targeting ligands can be attached to nanoparticles to improve tumor and cell-specific targeting.[1, 15] Similar strategies have been employed to target TAMs as well by leveraging overexpression of receptors consistent with the largely anti-inflammatory, pro-tumor phenotype.[16, 17] Sugar moieties have recently been revealed as promising targeting ligands to bring therapies to cancer cells and TAMs, which take advantage of the increased metabolism in the tumor.[18-22] These strategies target altered metabolism and receptor expression in cancer cells and TAMs to achieve drug delivery. In addition, sugars are highly water soluble and nontoxic, facilitating formulation and translation.

Dendrimer-based nanomedicines have shown great potential in targeting neuroinflammation and brain tumors.[23-32] Dendrimers are multivalent yet monodisperse and precise macromolecules which represent a promising nanoplatform for designing targeted drug delivery systems. We have previously shown that polyamidoamine (PAMAM) generation 4 hydroxyl-terminated dendrimers are able to cross the impaired blood-brain barrier upon systemic administration and selectively target activated microglia/macrophages in a variety of neurodegenerative diseases.[33-39] We have also shown in the context of cerebral palsy that mannose-modified dendrimers can alter the internalization pathway of dendrimers in activated glia.[34]

In the context of brain tumors, we have shown that hydroxyl PAMAM dendrimers provide dual advantages, to overcome blood-brain and solid tumor barriers from systemic administration and to specifically target TAMs and activated microglia.[24] Cancer cells demonstrate a switch away from oxidative phosphorylation and towards anaerobic glycolysis, termed the Warburg effect, where energy production is less efficient but significantly more rapid.[40, 41] Therefore, we envisioned that the surface modification with sugar molecules would enable dendrimers to broaden their TAMs targeting to directly target cancer cells as well. In this study, we explore the impacts of dendrimer

surface modification with sugars (glucose, mannose, or galactose) on tumor targeting in an orthotopic, immunocompetent model of glioblastoma. We demonstrate that surface decoration of these dendrimers with sugar moieties can significantly alter their interactions *in vivo*, with implications for designing tailored targeting systems in glioblastoma treatment.

Materials and Methods

Chemistry experiments:

Materials—Pharma grade generation 4 hydroxyl PAMAM dendrimer with ethylenediamine-core (64 hydroxyl terminal-groups, D-OH) was purchased from Dendritech in the form of methanolic solution. Methanol was removed under vacuo prior to use. Azido-PEG-4-amine was purchased from Broadpharm. 5-Hexynoic acid, 1-ethyl-3-(3-dimethylaminopropyl)carbodiimide (EDC), 4(dimethylamine)pyridine (DMAP), copper sulfate pentahydrate, sodium ascorbate was purchased from Sigma Aldrich US. Cy5 NHS ester was purchased from GE healthcare. All the solvents were purchased from Sigma and were used as received. Deuterated solvents for NMR were purchased from Sigma. The experiments were conducted in standard oven-dried glassware. The click reactions with sugar-azides were performed in the microwave reactor using microwave safe vials.

Synthetic protocols—β-D-Glucose-PEG4-azide, β-D-Galactose-PEG4-azide, and α-D-Mannose-PEG4-azide were synthesized using previously published protocol[34, 42] and were characterized using ^{1}H NMR spectroscopy (Supplementary Figure S1).

Synthesis of compound 3 (D-Hexyne): In an over-dried flask, compound 2 (5g, 0.35mmoles) was dissolved in anhydrous *N, N* dimethylformamide (DMF, 20mL). The solution was stirred and 5-hexynoic acid (980mg. 8.75mmoles) was added followed by the addition of DMAP (512mg, 4.2mmoles) and EDC (1.67g, 8.75mmoles). The stirring was continued at room temperature for 24 hours. The reaction was then diluted with DMF (100mL) and transferred to the dialysis membrane (1000Da cut off). The dialysis was first performed against DMF, followed by water until all the DMF was exchanged by the water. The water solution was then lyophilized to obtain the product as white solid (80% yield).

^{1}H NMR (500 MHz, DMSO) δ 8.09 – 7.74 (m, D-internal amide H), 4.71 (bs, D-OH), 4.02 (t, J = 5.5 Hz, ester $-CH_2$), 3.44-3.24 (m, dendrimer-CH_2), 3.10 – 3.03 (m, dendrimer-CH_2 and linker H), 2.81-2.57 (m, dendrimer-CH_2 and linker H), 2.48-2.34 (m, dendrimer-CH_2), 2.27-2.12 (m, dendrimer-CH_2), 1.71 (t, linker $-CH_2$). (Supplementary Figure S2A)

Synthesis of compound 5 (NH_2-D-hexyne): In an over-dried flask, compound 3 (5g. 0.316mmoles) was dissolved in anhydrous *N, N* dimethylformamide (DMF, 10mL). The solution was stirred and azido-PEG-4-amine (323mg, 1.26mmoles) was added dissolved in DMF (1mL). To the stirring reaction mixture, catalytic amount of $CUSO_4.5H_2O$ (40mg, 0.158mmoles) dissolved in water (1mL) was added followed by the addition of the catalytic amount of sodium ascorbate (31mg, 0.158mmoles) dissolved in water (1mL). The reaction mixture was stirred at 40°C overnight. The reaction was then brought to room temperature and diluted with water (100mL). A solution of ethylenediaminetetracetic acid (EDTA,

1mL) was added and dialysis was performed against water. The water solution was then lyophilized to obtain the product as white solid (82% yield).

^{1}H NMR (500 MHz, DMSO) δ 8.15-7.68 (m, D-internal amide H & PEG traizole H), 4.47 (t, triazole −CH_2), 4.01 (t, ester −CH_2), 3.80 (t, triazole −CH_2), 3.57-3.22 (m, PEG H, dendrimer-CH_2), 3.19 – 3.00 (m, dendrimer-CH_2), 2.82 – 2.57 (m, dendrimer-CH_2 and linker H), 2.43-2.32 (m, dendrimer-CH_2), 2.30-2.03 (m, dendrimer-CH_2), 1.83 (m, linker H), 1.69 (t, linker H). (Supplementary Figure S2B)

^{1}H NMR (500 MHz, MeOD) δ 7.76 (s, PEG traizole H), 4.46 (t, triazole −CH_2), 4.05 (t, ester −CH_2), 3.79 (t, triazole −CH_2), 3.63 – 2.97 (m, PEG H, dendrimer-CH_2), 2.84-2.58 (m, dendrimer-CH_2 and linker H), 2.41 – 2.05 (m, dendrimer-CH_2 and linker H), 1.87 (m, linker H), 1.70 (t, linker H) (Supplementary Figure S2C).

Synthesis of compound 6 (D-Sugar): To a stirring solution of compound 5 (1g, 0.06mmoles) in DMF (4mL) in a microwave-safe reaction vial, a solution of sugar azide (367.9mg, 0.96mmoles) in DMF (1mL) was added. This was followed by the addition of catalytic amount of $CuSO_4.5H_2O$ (15mg, 0.06mmoles) dissolved in water (1mL) and sodium ascorbate (12mg, 0.06mmoles) dissolved in water (1mL). The reaction was stirred in a microwave reactor (Biotage) at 50°C for 8 hours. The reaction was then brought to room temperature and diluted with water (100mL). A solution of ethylenediaminetetracetic acid (EDTA, 1mL) was added and dialysis was performed against water. The water solution was then lyophilized to obtain the product as white solid (80-90% yield).

D-Glucose, 6a:

^{1}H NMR (500 MHz, DMSO): δ 8.39 – 7.49 (m, dendrimer internal amide H + Triazole H), 4.50 – 4.42 (m, triazole-CH_2), 4.15 (d, J = 6.3 Hz, anomeric H glucose), 4.05 – 3.98 (m, linker CH_2 + glucose), 3.90 – 3.75 (m, glucose H), 3.69 – 2.85 (m, dendrimer +PEG + glucose H), 2.80 – 2.56 (m, dendrimer H), 2.40 – 2.15 (m, dendrimer H), 1.84 (s, hexynoic linker CH_2). (Supplementary Figure S3A)

^{1}H NMR (500 MHz, D_2O): δ 7.96 – 7.84 (m, triazole glucose + PEG H), 4.63 – 4.55 (m, triazole-CH_2), 4.48 (d, J = 7.1 Hz, glucose anomeric H), 4.08 −4.02 (m, glucose H), 4.05 – 3.88 (m, linker CH_2 + glucose), 3.86 – 3.23 (m, dendrimer +PEG + glucose H), 3.08 – 2.29 (m, dendrimer H), 2.02 – 1.89 (m, hexynoic linker CH_2). (Supplementary Figure S3B)

D-Galactose, 6b:

^{1}H NMR (500 MHz, DMSO): δ 8.18 – 7.58 (m, dendrimer internal amide H + triazole H), 4.46 (s, triazole-CH_2), 4.13 – 4.02 (m, galactose CH_2), 4.03 – 3.98 (m, dendrimer CH2 + galactose H), 3.85 – 3.77 (galactose H), 3.65 – 3.35 (m, dendrimer + PEG H), 3.34 – 3.17 (dendrimer H), 3.14 −3.05 (dendrimer H), 2.91 – 2.88 (m, dendrimer H), 2.75 – 2.58 (m, dendrimer H), 2.44 – 2.05 (m, dendrimer H), 1.83 (s, hexynoic acid linker CH_2). (Supplementary Figure S4A)

^{1}H NMR (500 MHz, D_2O): δ 7.93 (br s, PEG-4 triazole, 3H), 7.86 (br s, galactose triazole, 13H), 4.60 – 4.55 (m, CH_2-triazole, 30H), 4.42 (d, J = 7.4 Hz, galactose anomeric H), 4.16

– 4.12 (m, galactose H), 4.07 – 4.04 (m, galactose H), 3.96 – 3.88 (m, dendrimer-galactose H), 3.85 – 3.48 (m, dendrimer-galactose H), 3.47 – 3.43 (m, galactose H), 3.35 – 3.26 (m, dendrimer H), 3.02 – 2.99 (m, dendrimer H), 2.97 – 2.58 (m, dendrimerH), 2.44 (s, dendrimerH), 1.99 – 1.90 (m, CH2-hexynoic acid linker). (Supplementary Figure S4B)

D-Mannose, 6c:

^{1}H NMR (500 MHz, DMSO): δ 8.15 – 7.75 (m, dendrimer internal amide H + triazole H), 4.64 – 4.61 (m, mannose anomeric H), 4.49 – 4.44 (m, triazole-CH_2), 4.04 – 3.93 (m, linker CH_2), 3.7 – 3.3 (m, dendrimer + glucose + PEG H), 3.71 – 3.19 (m, dendrimer H), 3.18 – 3.00 (m, dendrimer H), 2.66 – 2.56 (m, dendrimer H), 2.45– 2.04 (m, dendrimer H), 1.87 – 1.79 (m, hexynoic linker CH_2). (Supplementary Figure S5A)

^{1}H NMR (500 MHz, D_2O): δ 7.93 br (s, PEG triazole H), 7.86 (br s, mannose triazole H), 4.61 – 4.55 (m, triazole-CH_2), 4.40 (d, J = 7.4 Hz, mannose anomeric H), 4.18 – 4.02 (m, mannose H), 3.97 – 3.88 (m, linker CH_2 + mannose H), 3.85 – 3.41 (m, dendrimer + mannose +PEG H), 3.37 – 3.27 (m, dendrimer H), 3.30 – 2.30 (m, dendrimer H), 2.50 – 2.35 (m, dendrimer H), 1.98 – 1.90 (m, hexynoic linker CH_2). (Supplementary Figure S5B)

Synthesis of compound 7 (Cy5-D-Sugar): In an over-dried flask, compound 6 (50mg. 0.0023mmoles) was dissolved in anhydrous *N, N* dimethylformamide (DMF, 4mL). The solution was stirred and the pH was brought to 7.4 using DIPEA. This was followed by the addition of Cy5-NHS ester (5mg, 0.007mmoles). The reaction was stirred at room temperature for 12 hours, protected from light. The reaction was then diluted with DMF (50mL) and transferred to the dialysis membrane (1000Da cut off). The dialysis was first performed against DMF, followed by water dialysis until all the DMF is exchanged by the water. The water solution was then lyophilized to obtain the product as blue solid which was further purified on G-25 sephadex column (65-75% yield).

NMR (Cy5-D-Glucose, 7a): ^{1}H NMR (500 MHz, DMSO) δ 8.42 – 8.33 (m, Cy5 H), 8.20 – 7.68 (m, dendrimer internal amide H + triazole H), 7.68 – 7.61 (m, Cy5 H), 7.35 – 7.30 (m, Cy5 H), 6.35 −6.27 (m, Cy5 H), 5.03 – 4.87 (m, glucose H), 4.80 – 4.65 (m, dendrimer OH), 4.49 (m, triazole-CH_2), 4.20 – 3.92 (m, glucose +dendrimer linker CH_2), 3.90 – 3.74 (m, glucose H), 3.69 – 2.89 (m, dendrimer + glucose +PEG H), 2.80 – 2.60 (m, dendrimer H), 2.46 – 2.10 (m, dendrimer H), 1.89 – 1.79 (m, dendrimer H), 1.71 – 1.14 (m, Cy5 H and linker H). (Supplementary Figure S6A; HPLC: Purity >99%, Retention time: 12.83 min. (Supplementary Figure S7A).

^{1}H NMR (Cy5-D-Galactose, 7b): ^{1}H NMR (500 MHz, DMSO) δ 8.36 (t, J=12.7 Hz, Cy5 H), 8.12 – 7.72 (m, dendrimer internal amide H + triazole H), 7.66 – 7.58 (m, Cy5 H), 7.36 – 7.26 (m, Cy5 H), 6.62 −6.53 (m, Cy5 H), 4.87-4.40 (m, galactose H), 4.36 (m, triazole-CH_2), 4.19 – 3.71 (m, glucose +dendrimer linker CH_2), 3.66 – 2.96 (m, dendrimer + galactose +PEG H), 2.78 – 2.55 (m, dendrimer H), 2.44 – 2.05 (m, dendrimer H), 1.89 – 1.74 (m, dendrimer H), 1.73 – 1.12 (m, Cy5 H and linker H). (Supplementary Figure S6B); HPLC: Purity >99%, Retention time: 13.02 min. (Supplementary Figure S7B).

^{1}H NMR (Cy5-D-Mannose, 7c): ^{1}H NMR (500 MHz, DMSO) δ 8.37 (t, *J* = 12.1 Hz, Cy5 H), 8.15 – 7.75 (m, dendrimer internal amide H + triazole H), 7.67 – 7.61 (m, Cy5 H), 7.33 – 7.27 (m, CY5 H), 6.33 – 6.26 (m, CY5 H), 4.85 – 4.55 (m, mannose H + OH + dendrimer OH), 4.50 – 4.38 (m, triazole-CH_2), 4.17 – 3.93 (m, m, linker CH_2 + mannose H), 3.75 (m, mannose H), 3.71 – 3.23 (m, dendrimer + mannose +PEG H), 3.16 – 3.03 (m, dendrimer H), 2.65 – 2.55 (m, dendrimer H), 2.47 – 2.07 (m, dendrimer H), 1.84 (m, m, hexynoic linker CH_2), 1.72 – 1.10 (m, Cy5 H and linker H). (Supplementary Figure S6C); HPLC: Purity >99%, Retention time: 12.97 min. (Supplementary Figure S7C).

Instrumentation for characterization of intermediates and dendrimer conjugates—The structures of intermediates and dendrimer conjugates were analyzed using proton nuclear magnetic resonance (^{1}H NMR) spectroscopy. NMR spectra were recorded on a Bruker spectrometer (500 MHz) at ambient temperatures. The NMR data is presented as chemical shift values (δ ppm) and multiplicity. The chemical shifts of the residual protic solvent such as $CDCl_3$ ^{1}H, δ 7.27 ppm), D_2O ^{1}H, δ 4.79 ppm); and DMSO-*d*6 ^{1}H, δ2.50 ppm) were used for chemical shifts calibration. The purity of the final dendrimer conjugates was evaluated using high pressure liquid chromatography (HPLC). HPLC was run on a Waters Corporation system equipped with 2998 photodiode array detector and a 2475 multi λ fluorescence detector. The instrument had an in-Line degasser, and a 1525 binary pump. The chromatogram were analyzed using Waters Empower 2 Software. The dendrimer samples were run through a C18 Waters column (C18 symmetry 300, 5μm, 4.6x250mm) maintaining the flowrate at 1.0 mL/min. A gradient flow method was used using 0.1% TFA and 5% acetonitrile in water (A) and 0.1% TFA in acetonitrile (B). The method started from a gradient 90:10 (A:B), stayed at 90:10 (A:B) for 3 minutes, gradually increasing to 50:50 (A:B) at 16 minutes, stayed at 50:50 (A:B) at 25 minutes, and finally returned to 90:10 (A:B) at 35 minutes. The chromatogram were monitored at wavelengths 210 (dendrimer absorption) and 650 nm (Cy5 absorption). The particle size distribution and zeta potential distribution of dendrimer conjugates were measured via Dynamic light scattering on a Malvern Zetasizer Nano ZS instrument using previously our previously published protocols.[34]

Biology experiments:

Materials—Bovine serum albumin (BSA), 4-[[[[4-(1,1-Dimethylethyl)phenyl]sulfonyl]amino]methyl]-N-3-pyridinylbenzamide (STF-31), and α-lactose were obtained from Sigma Aldrich (St. Louis, MO, USA). Dulbecco's modified eagle medium (DMEM), Roswell Park Memorial Institute (RPMI) media, L-glutamine, fetal bovine serum (FBS), penicillin-streptomycin (P/S) antibiotic, 0.25% trypsin-EDTA, normal goat serum (NGS), goat anti-rabbit Alexafluor 488, and (3-(4,5-dimethylthiazol-2-yl)-2,5-diphenyl tetrazolium bromide) MTT reagent were purchased from Invitrogen (Carlsbad, CA, USA). Tris-buffered saline (TBS) and phosphate buffered saline (PBS) were purchased from Corning (Corning, NY, USA). Ionized calcium binding adaptor molecule (Iba1) primary antibody was purchased from Wako Pure Chemical Corporation (Tokyo, Japan). NucBlue cell stain (DAPI) was purchased from Cell Signaling (Danvers, MA, USA). Methanol was purchased from ThermoFisher (Waltham, MA, USA). Recombinant murine interleukin 4 (IL4) was obtained from Peprotech Inc. (Rocky Hill, NJ, USA).

Tumor Inoculations—GL261 murine microglia were obtained from the DTP/DCTD/NCI Tumor Repository (National Cancer Institute, Frederick, MA, USA). Cells were cultured in RPMI supplemented with 10% FBS, 1% P/S, and 1% L-glutamine and maintained at 37°C and 5% CO_2 atmosphere. All animals were housed at Johns Hopkins University animal facilities and given free access to food and water. Experiments performed were approved by the Johns Hopkins Institutional Animal Care and Use Committee. Male and female C57BL/6 mice were obtained from Jackson Laboratory Company (Bar Harbor, ME, USA). Mice 6-8 weeks old were inoculated with glioblastoma tumors via intracranial injection of GL261 cells. Mice were anesthetized with a ketamine/xylazine cocktail for surgeries. An incision was created in the center of the scalp. A burr hole was drilled at 1 mm posterior to the bregma and 2 mm lateral to the midline for injection into the striatum in the right hemisphere. A 2 μL injection of 100,000 GL261 cells were injected to a depth of 2.5 mm over 10 min with a stereotactic frame and automated syringe pump (Stoelting Co., Wood Dale, IL, USA). The syringe was withdrawn, and the incision sutured (Ethicon Inc., Somerville, NJ, USA).

Immunohistochemistry and confocal microscopy—On day 14 post-inoculation, glioblastoma bearing mice were intravenously injected with unmodified hydroxyl-terminated dendrimers, dendrimer-glucose, dendrimer-mannose, or dendrimer-galactose conjugates at 55 mg/kg on the whole conjugate basis. At this time point, tumors exhibit an average mass of 34.0 ± 6 mg. 24 hours after injection, brains, livers, and kidneys were collected and fixed overnight in 4% formalin solution (n=2 per construct). Organs were then passed through a sucrose gradient (10%, 20%, then 30% sucrose in PBS overnight each) to remove formalin. Brains were sectioned axially into 30 μm slices with a Leica CM 1905 cryostat (Wetzlar, Germany). Brains were stained for DAPI to visualize nuclei and Iba1 (1:200) to visualize tumor-associated macrophages. Kidneys were stained for GFAP (1:500) to visualize tubules. Livers were stained for serum albumin (1:1000, Abcam) to visualize hepatocytes or SE-1 (1:200, Novus Biologicals) to visualize sinusoidal endothelial cells. Images were acquired on a Zeiss LSM710 confocal microscope (Hertfordshire, UK). Image capture settings and processing adjustments were kept constant across all compared images with different dendrimer types.

Dendrimer tissue extraction and quantification—At specified time points (1, 4, 24 hours) after administration, animals were euthanized and perfused with saline to remove residual blood in organs. Organs and plasma were collected and snap frozen in liquid nitrogen (n=5 per construct). To assess tumor targeting, tumors and healthy brain tissue from the contralateral hemisphere were dissected out. Tissues were dissected (100 mg for livers and kidneys, 50 mg for hearts and lungs, 20 mg for spleens) for dendrimer extraction. Tumors were homogenized and quantified whole and presented as μg/g tissue to normalize for tumor size. Tissue samples were homogenized in methanol at 100 μL per 100 mg with stainless steel homogenization beads (Next Advance, Troy, NY, USA), followed by sonication for 15 minutes. Samples were spun down at 12,000 rpm and supernatants collected for analysis. Plasma samples were diluted 5x in PBS and filtered through a 0.2 μm filter. For quantification, dendrimer solutions were read on a Shimadzu RF-3501 spectrofluorophotometer (Kyoto, Japan). Control samples of brain tumors without

dendrimer administration were used to correct for tissue background fluorescence. The wavelengths used for the Cy5 labeled conjugates were excitation 645 nm and emission 662 nm. Calibration curves for each dendrimer of known concentrations were created to convert measured intensities to tissue concentrations. Tumor specificity was calculated as the ratio of dendrimer content within the tumor divided by content in the contralateral hemisphere. To explore dendrimer-glucose blood brain barrier penetration, healthy mice were intravenously injected with dendrimer, collected 24 hours later, and processed as described above.

In vitro dendrimer uptake experiments—BV2 murine microglia and GL261 murine glioblastoma cells were maintained in incubators at 37°C and 5% CO_2 atmosphere. BV2 cells were grown in DMEM supplemented with 10% FBS and 1% P/S. GL261 cells were grown in RPMI supplemented with 10% FBS, 1% P/S, and 1% L-glutamine. Treatments were performed in half serum media (5% FBS). Cell viabilities for each dendrimer conjugate were measured using MTT assay as per manufacturer's procedure.

To explore dendrimer-glucose cell interactions, BV2 microglia were treated with 50 μg/mL unmodified or glucose conjugated dendrimers. For blocking experiments, cells were exposed to STF-31 at 10 μM for 24 hours to block GLUT-1 transporters, followed by incubation with dendrimers for 6 hours. For cellular internalization, BV2 cells were incubated with unmodified and glucose dendrimers for 24 hours in the absence or presence of IL4. Cells were then collected in methanol, dendrimer extracted, and quantified on the spectrofluorophotometer as described above for tissues. For dendrimer uptake in GL261 cells, tumor cells were incubated with 10 μg/mL of each dendrimer for 24 hours. Cells were then washed, collected, and homogenized as described. To explore dendrimer-galactose cell interactions, GL261 glioblastoma cells were incubated with unmodified or galactose dendrimers for 24 hours in the presence or absence of α-lactose at 100 μM to block galectins. Membrane and cytosolic fractions were separated using the Mem-PER Plus protein extraction kit (ThermoFisher) and measured using the spectrofluorophotometer.

Statistical analyses—Statistical analyses and graphs were created using GraphPad Prism v8.0 software (San Diego, CA, USA). All error bars presented in figures show mean ± standard errors. Statistical significances between dendrimer types in biodistribution were calculated using two-way ANOVAs. Differences between groups in *in vitro* experiments were performed using Student's t-tests.

Results and Discussion

Synthesis of dendrimer-sugar conjugates

Glycosylation of nanoparticles have attracted significant interest in the development of targeted drug delivery systems due to their specific ligand-receptor recognition. Since sugars are natural targeting ligands and are integral part of several biological processes in human body, their incorporation into nanoparticles provide stealth without compromising their cellular uptake, biocompatibility, non-immunogenicity and enhance their blood circulation time and enzymatic stability in the serum.[43, 44] Moreover, sugar units are synthetically appealing for functionalization of nanocarriers and can be easily modified specifically at the anomeric position for the attachment of linkers.[43] To assess how surface decoration

with sugars impacts dendrimer *in vivo* transport and targeting properties in glioblastoma model, we synthesized generation 4 hydroxyl-terminated PAMAM dendrimers conjugated to β-D-glucose, β-D-galactose, or α-D-mannose via click chemistry approach (Figure 1A). In recent years, click chemistry has been a powerful tool to create libraries of small molecules, synthesis of complex macromolecules and for the surface conjugation of polymers and dendrimers. [45, 46] Sugars were modified with a short PEG linker to reduce steric hindrance to receptor interactions. This sugar linker was then attached to the dendrimer surface via copper catalyzed azide-alkyne click (CuAAC) reaction to produce sugar dendrimer conjugates. The synthesis began with the construction of clickable glucose, galactose & mannose-azides (**1a,b,c**) using our previously published protocols (Figure 1B). On the other hand, the alkyne-terminating clickable dendrimer was synthesized by partial modification of 14-16 OH groups on the surface of dendrimer (D-OH, **2**). These hydroxyl groups were esterified with 5-hexynoic acid using EDC/DMAP coupling chemistry to afford D-hexyne (**3**). 3-4 arms of alkyne groups on D-hexyne were clicked with azido-PEG-4amine (**4**) to generate a trifunctional dendrimer (NH_2-D-hexyne, **5**) with ~12 alkyne and ~3-4 amine functional groups. The alkyne terminal groups were meant to participate in CuAAC reaction with azide terminating sugars while amine surface groups will be utilized for the attachment of near infra-red dye cyanine 5 (Cy5) for imaging purpose. The dendrimer (**5**) was reacted with sugar-azides (**1**) (β-D-Glucose-PEG4-azide, β-D-Galactose-PEG4-azide, and α-D-Mannose-PEG4-azide) using CuAAC reaction in the presence of catalytic amounts of copper sulphate pentahydrate and sodium ascorbate to yield corresponding dendrimer-sugar conjugates (**D-Sugar, 6**). The dendrimer-sugar conjugates were purified in the presence of ethylenediaminetetraacetic acid (EDTA) using tangential flow filtration to remove excess of reagents and the traces of copper. Use of click chemistry enabled a precise control of sugar payload on the dendrimer. We utilized only12-14 hydroxyl groups on the dendrimer surface for the attachment of sugar moieties to maintain the inherent brain tumor targeting properties of hydroxyl PAMAM dendrimers (nearly neutral surface charge; ~5nm) while exploring the effect of various sugars as targeting ligands. We have previously shown that the surface modification up to 20 wt% does not alter the properties of dendrimers to target neuroinflammation and brain tumor.[27, 38, 47] The amine groups in each of the D-Sugar conjugates were reacted with Cy5-mono-NHS ester at pH7.5-8 to obtain fluorescently labeled **Cy5-D-Sugars [Cy5-D-Glucose (7a); Cy5-D-Galactose** (7b); and **Cy5-D-Mannose** (7c)].

Characterization and chemical validation of dendrimer sugar conjugates

Throughout the synthesis of fluorescently labeled **D-Sugar** conjugates, we analyzed the structures at every step via ^{1}H NMR spectroscopy (Figure 2). The synthesis of D-Hexyne (**3**) is confirmed by the appearance of ester methylene proton at δ 4.0 ppm and a methylene proton from hexyne linker at δ 1.7 ppm (Figure 2A). The number of hexyne linkers conjugated in the surface of the dendrimer were calculated by comparing the integration of dendrimer internal amide protons to ester methylene protons, which revealed −14-16 linkers were attached. HPLC showed a shift in retention time from D-OH at 9.5 min to D-Hexyne at 13.4 min. The success of the partial click with amine terminating PEG linker was analyzed by the appearance of triazole methylene protons (Figure 2B) and the triazole proton at δ 7.76 ppm when NMR was taken in methanol to exchange dendrimer amide

protons (Supplementary Figure S2C). The presence of a few amine groups resulted in a shift in retention time on HPLC at 9.6 min. The NMR spectra of resulting D-Sugars after click reaction with sugar-azides clearly showed the presence of proton signals from glucose, galactose and mannose along with other dendrimer signals (Figures 2C-E). To confirm the success of click reaction, the NMRs were also taken in D_2O. The deuterium exchange resulted in the disappearance of internal amide protons revealing two distinct peaks corresponding to the triazole protons from two different click reactions (Supplementary Figure S3B, S4B and S5B). The resulting dendrimer-sugar conjugates were highly pure (>99% purity) as analyzed by the HPLC (Figure 3A). Remarkably tight loading of ~12 molecules of sugars in each conjugate was evident from ^1H NMR and HPLC showing click reaction as a stupendous tool for the ligation on the surface of macromolecules. Upon Cy5 labeling, appearance of Cy5 protons in aromatic, allyl and aliphatic regions were evident from the NMR spectra and confirmed the attachment of 1-2 molecules of Cy5 in all three conjugates (Figures 2F-H and Supplementary Figure S6). The HPLC purity at 650nm (Cy5 absorbance) showed highly pure dendrimers with purity greater than 99% (Supplementary Figure S7). The tumor targeting potential of hydroxyl PAMAM dendrimers is due to their small size and nearly neutral zeta potential. We further measured the hydrodynamic diameter and zeta potential of **D-sugars** to evaluate the effect of sugar conjugation. The size distribution by number and zeta potential distribution are presented in Figure 3B and 3C. The sugar conjugation resulted in a slight increase in the size from **D-OH** (~4nm) to −5 nm for **D-Sugars**. The sizes of **D-GLU**, **D-GAL**, and **D-MAN** were 4.79nm, PDI: 0.48; 4.53nm, PDI: 0.49; and 4.97nm, PDI: 0.52 respectively. The zeta potential was nearly neutral for all three dendrimer-sugar conjugates in the range from 7-10 mV.

Localization of sugar dendrimer conjugates in vivo in orthotopic brain tumors

To assess impacts of sugar dendrimer conjugation on *in vivo* trafficking, glioblastoma brain tumor bearing mice were injected intravenously with fluorescently labeled (unmodified Cy5 dendrimer (**D-OH**), Cy5-D-glucose- (**D-GLU**), Cy5-D-mannose- (**D-MAN**), or Cy5-D- galactose (**D-GAL**) dendrimers. Dendrimers were administered 14 days after tumor inoculation, and brains were collected for imaging 24 hours post-injection. Brains were then stained with DAPI to visualize cell nuclei and lectin (*Lycopersicon Esculentum* lectin) to label TAMs and microglia.

Consistent with our previous studies, **D-OH** is able to overcome brain and solid tumor barriers to selectively localize within TAMs and activated microglia (Figure 4). **D-OH** exhibited perinuclear signal pattern within these cells. **D-GLU** and **D-MAN** exhibited the same TAMs and microglia targeted signal, indicating that the dendrimer transport properties are preserved, upon sugar modification. Mannose receptors (CD206) are highly upregulated on anti-inflammatory, pro-tumor macrophages and have been leveraged in TAMs targeting platforms.[18, 48] Therefore, the TAMs targeting of **D-MAN** was expected. However, **D-GLU** also exhibited the same TAMs and microglia targeting, which was a surprising result. Glucose has been explored to bring therapies directly to cancer cells by leveraging the altered metabolism exhibited by cancer cells.[49, 50] However, **D-GLU** exhibited the same TAMs and microglia targeting as **D-OH**, indicating that glucose moieties are insufficient to overcome dendrimer affinity for TAMs and microglia. In addition, macrophages have

also been shown to exhibit upregulated glucose transporters in the context of inflammation.[51] **D-GAL** exhibited highly distinct signal pattern separate from **D-OH** and other sugar modified dendrimers (Figure 4). While some signal was observed in TAMs and microglia, **D-GAL** primarily exhibited highly punctated signal pattern in the tumor microenvironment. We theorize that this signal pattern arises from **D-GAL** interactions with galectins on the surface of cancer cells. Galectins are highly overexpressed in many cancers, including glioblastoma, and have been shown to regulate cell interactions with the extracellular matrix to mediate cancer cell invasion and metastasis. [52, 53]

Sugars may also interact with receptors on other cell types in peripheral organs. To explore off-target interactions after systemic administration, unmodified and sugar dendrimers were injected intravenously into brain tumor bearing mice. 24 hours after injection, kidneys and livers were collected and stained for confocal imaging. Kidneys were stained with DAPI to label nuclei and GFAP to label proximal tubules (Supplementary Figure S8). Livers were stained with DAPI to label nuclei and serum albumin to label hepatocytes or SE1 to label sinusoidal endothelial cells (Supplementary Figure S9A, B). **D-OH** exhibited high localization within renal proximal tubules, consistent with nanoparticle clearance via kidney fenestrations in this size range.[54] **D-GLU**, **D-MAN**, and **D-GAL** exhibited similar signal localization within the tubules, indicating that the primary clearance route of dendrimers is not altered with sugar surface decoration. In the kidneys, **D-OH** exhibits minimal signal lining the portal veins, indicating negligible liver accumulation. In contrast, **D-GAL** exhibits broad signal throughout the liver targeted to hepatocytes (Supplementary Figure S9A). This is consistent with established reports that hepatocytes exhibited high expression of asialoglycoprotein receptors, which bind with galactose.[55] This hepatocyte targeting has implications for targeting liver diseases and has been used for targeted delivery in liver diseases and hepatic cancers.[56, 57] **D-GLU** and **D-MAN** exhibited signal localized to within sinusoidal endothelia (Supplementary Figure S9B).[58] This indicates that in addition to renal clearance, **D-GLU** and **D-MAN** may also be experiencing clearance from the body via liver filtration. This is consistent with previous reports where mannose receptor mediates uptake by sinusoidal endothelial cells for clearance.[59] Surprisingly, despite receptors for these sugars being implicated in Kupffer cell internalization,[60] no uptake in Kupffer cells was observed with these sugar dendrimers, indicating that the risk of off-target immune modulation with these sugar dendrimers in the liver is minimal.

Quantification of tumor accumulation by sugar dendrimer conjugates

To quantify tumor accumulation, brain tumor bearing mice were intravenously injected with unmodified or sugar-modified dendrimers on day 14 after tumor inoculation. Brains and organs were then collected at specified time points, extracted for dendrimers, and quantified with fluorescence quantification.

D-GLU exhibited ~8-fold higher tumor accumulation compared to unmodified dendrimer (Figure 5A, $p < 0.001$ **D-OH** vs. **D-GLU**). At 24 hours after injection after equivalent dose of dendrimers administered, **D-GLU** exhibited 15.0±4.7 μg/g tissue compared to unmodified **D-OH** which exhibited 1.9 ±0.3 μg/g tissue in the tumor. **D-GLU** exhibited similar tumor accumulation compared to generation 6 unmodified dendrimers, which

experience size-dependent longer circulation time due to decreased renal clearance rate.[24] **D-MAN** and **D-GAL** altered the kinetics of dendrimer tumor targeting, shifting the peak from 4 hours earlier to 1 hour post-injection ($p = 0.072$ **D-OH** vs. **D-MAN**, $p = 0.0013$ **D-OH** vs. **D-GAL**). **D-MAN** and **D-GAL** exhibited ~2- and ~2.5-fold greater tumor accumulation at 1 hour compared to D-OH, but cleared faster from the tumor and exhibited ~50% lower levels within the tumor after 24 hours compared to **D-OH**. These trends are similar to *in vitro* dendrimer internalization into GL261 tumor cells (Supplementary Figure S10), with **D-GLU** exhibiting ~10-fold greater internalization than the other dendrimers. Notably, all sugar-modified dendrimers significantly improved dendrimer specificity for the brain tumor compared to healthy brain tissue of the contralateral hemisphere (Figure 5B, $p = 0.0007$ **D-OH** vs. **D-GLU**, $p = 0.0012$ **D-OH** vs. **D-MAN**, $p = 0.001$ **D-OH** vs. **D-GAL**). **D-OH** exhibited a tumor/contralateral hemisphere ratio of 3.4±1.0 24 hours after administration, while **D-GLU** exhibited 18.8±5.4, **D-MAN** exhibited 4.0±0.4, and **D-GAL** exhibited 7.1±1.7. Compared to quantification of liposomal nanoparticle tumor targeting in an orthotopic brain tumor model, **D-GLU** demonstrated ~100-fold greater tumor accumulation, while **D-MAN** and **D-GAL** exhibited ~8-fold greater tumor accumulation.[61] **D-GAL** and **D-MAN** performed similarly to gold [62, 63] and PEGylated iron oxide[64] nanoparticles, while **D-GLU** exhibited ~10-fold greater tumor accumulation. Specificity for the tumor of these sugar-modified dendrimers also compared favorably to other nanoparticles.[64, 65] In addition, these **D-GLU** and **D-MAN** exhibited highly specific localization within TAMs and activated microglia while **D-GAL** targeted the tumor extracellular space, whereas quantitative nanoparticle accumulation studies do not explore cell-type localization.[7] Therefore, these dendrimers can be applied for targeted, highly specific tumor targeting. Even though many nanoparticles are known to show a high accumulation into the tumor by the enhanced permeability and retention effect, this does not translate to intracellular accumulation.[7] In addition, the higher TAM intracellular accumulation of glucose-modified dendrimer could enable localized TAM immune programming from systemic administration.

Modification of dendrimers with sugars moderately alters systemic biodistribution

To evaluate impacts on off-target accumulation, we also compared organ accumulation of sugar-modified dendrimers to **D-OH** (Figure 6). All dendrimers are rapidly cleared from circulation, with less than 1% of the injected dose per mL plasma remaining in circulation 24 hours after injection (Figure 6A). **D-GLU** exhibited similar kidney levels to **D-OH**, while **D-MAN** and **D-GAL** were cleared significantly more rapidly from kidneys than **D-OH** (Figure 6B, $p < 0.0001$ **D-OH** vs. **D-MAN**, $p = 0.0004$ **D-OH** vs. **D-GAL**). Sugar dendrimers did exhibit significantly increased accumulation within the livers compared to **D-OH**, with **D-OH** exhibiting 0.29 ± 0.04 μg/g tissue, **D-GLU** exhibiting 7.8±3.0 μg/g tissue, **D-MAN** exhibiting 1.7±0.30 μg/g tissue, and **D-GAL** exhibiting 10.5±2.0 μg/g tissue. Consistent with these findings, glucose transporters with high uptake rates have been found in the liver. [66] Significantly increased liver accumulation was also expected with **D-GAL**, which targets galactose receptors on hepatocytes for implications in delivery to liver diseases.[67] Notably, despite increased liver accumulation, these sugar-modified dendrimers still exhibit lower liver content compared to free chemotherapies and other

nanoparticles with systemic administration. [68, 69] Sugar dendrimers also exhibited altered kinetics in the spleen, with **D-MAN** accumulating more slowly and **D-GAL** exhibiting significantly lower spleen accumulation (Figure 6D, $p = 0.0143$ **D-OH** vs. D-MAN, $p < 0.0001$ **D-OH** vs. **D-GAL**). Notably, **D-GLU** exhibited significantly greater accumulation in lungs (Figure 5E, $p = 0.0002$ **D-OH** vs. **D-GLU**) and hearts (Figure 6F, $p = 0.003$ **D-OH** vs. **D-GLU**). This is consistent with findings where lungs and hearts uptake glucose due to high energy demands.[70, 71]

Glucose-conjugated dendrimer increases cellular internalization and BBB penetration

We have previously shown that dendrimer surface decoration with mannose moieties alters the dendrimer internalization pathway from fluid-phase endocytosis to mannose receptor-mediated uptake but did not alter the overall magnitude of dendrimer internalization compared to unmodified dendrimers.[34] To confirm that **D-GLU** similarly interacted with the expected receptor and to explore how the significantly increased tumor accumulation arises, we investigated **D-GLU** uptake in BV2 murine microglia. To check cytotoxic effects, sugar dendrimers were first assessed for cell viability in microglia *in vitro* after 24 hours of exposure. Sugar dendrimers did not exhibit any cytotoxicity apart from slight toxicity with **D-GAL** at high dose, consistent with previous findings where galactose may induce toxicity in brain tissue at high concentrations (Supplementary Figure S11).[72]

STF31, an inhibitor of GLUT1, was used to block interactions with glucose. In the presence of STF31, **D-GLU** exhibited a significant decrease of ~20% in cellular internalization while **D-OH** exhibited a slight nonsignificant decrease of ~5% (Figure 7A, $p = 0.0083$ **D-GLU** - STF31 vs. **D-GLU** +STF31, $p = 0.13$ **D-OH** −STF31 vs. **D-OH** +STF31). This ~20% in internalization may be due to other glucose transporters, which can compensate for STF31 inhibition of GLUT1 to mitigate inhibition of cellular internalization of **D-GLU**. [73] These results indicate that conjugation of glucose to the dendrimer surface alters the internalization pathway towards glucose transporters. This interaction with glucose transporters significantly increased internalization of dendrimers in both resting and IL4 activated TAMs-like microglia (Figure 7B, $p = 0.0003$ −IL4 **D-GLU** vs. **D-OH**, $p = 0.0004$ +IL4 **D-GLU** vs. **D-OH**). **D-OH** exhibited a ~2-fold increase in internalization between resting and TAMs ($p = 0.016$ −IL4 **D-OH** vs. +IL4 **D-OH**) while **D-GLU** did not, indicating that **D-GLU** targets glucose transporters for enhanced internalization in a phenotype-independent manner. This is consistent with previous reports where GLUT1 expression is impacted by pro-inflammatory phenotype but remains unchanged with anti-inflammatory (pro-tumor) activation,[74] while IL4 stimulation induces increased endocytosis.[75] We have also previously demonstrated that **D-OH** internalization is enhanced in pro-inflammatory activated microglia.[76] We then looked at **D-GLU** brain accumulation in healthy mice to see if glucose modification impacted dendrimer BBB penetration. In healthy mice, **D-GLU** exhibited significantly increased brain penetration compared to **D-OH** consistent with levels observed in the contralateral hemisphere in brain tumor bearing mice (Figure 7C, $p = 0.0012$ **D-GLU** healthy vs. **D-GLU** CH, $p = 0.143$ **D-GLU** healthy vs. **D-OH** healthy). We hypothesized this increased penetration could be due to the interactions with glucose receptors on endothelial cells of the blood brain barrier, which transport nutrients into the brain for normal brain functions but warrants further

investigation.[77] Taken together, these results suggest that the significantly increased tumor accumulation exhibited by **D-GLU** is due to interactions with glucose receptors leading to significantly increased cellular internalization within TAMs.

Galactose-conjugated dendrimers interact with galectins for tumor cell surface targeting

D-GAL exhibited significantly altered signal pattern within the glioblastoma tumor compared to unmodified and other sugar modified dendrimers. Galectins are highly upregulated on cancer cell membranes and mediated interactions with the tumor extracellular matrix.[78] To determine if **D-GAL** was enabling interactions with galectins, GL261 murine glioblastoma cells were exposed to **D-GAL** or **D-OH** in the presence or absence of α-lactose, an broad inhibitor of galectins. [79] Membrane and cytosolic fractions of these treated GL261 cells were then separated. **D-GAL** exhibited significantly greater association with cell membranes than **D-OH**, and this interaction was inhibited in the presence of α-lactose (Figure 7D, $p = 0.027$ **D-GAL** −α-lactose vs. **D-OH** −α-lactose, $p = 0.0095$ **D-GAL** −α-lactose vs. **D-GAL** +α-lactose). **D-OH** exhibited no change in membrane association in the presence or absence of α-lactose. This confirms that conjugation of galactose moieties to the dendrimer surface enables interactions with galectins on glioblastoma cell membranes. Interestingly, **D-GAL** exhibited no change in the cytosolic fraction compared to **D-OH** and in the presence or absence of α-lactose, consistent with previous reports of galectins as mediators of extracellular matrix interactions rather than as internalization pathways (Figure 7E). These results indicate that **D-GAL** shifts dendrimer targeting away from TAMs and towards glioblastoma cell membranes by interacting with galectins, with implications for intratumor drug delivery, apart from immunotherapies.

Conclusion

Developments in nanotechnology are providing critically needed tumor-specific, intracellular targeted drug delivery strategies to improve patient outcomes in glioblastoma and other cancers. In this study, we explored three dendrimers precisely modified with glucose, mannose, or galactose sugar moieties as targeting ligands using click chemistry. We demonstrated that by conjugating mannose, glucose, or galactose to the dendrimer, we can significantly increase their tumor specificity with systemic administration and alter the kinetics of their tumor accumulation. In addition, these sugar moieties conferred receptor-specific interactions. **D-GLU** exhibited interactions with glucose transporters on TAMs, resulting in significantly increased TAMs specific tumor accumulation. **D-GAL** exhibited interactions with galactins on the surface of cancer cells, enabling targeting of the tumor microenvironment. Taken together, these results indicate that the dendrimer is an effective, highly versatile drug delivery platform that can be modified with targeting ligands to tailor their receptor interactions that take advantage of the unique tissue biophysics of hydroxyl dendrimers. Future work will focus on how these altered interactions can be leveraged to enhance the delivery of anti-cancer therapies for the treatment of glioblastoma.

Supplementary Material

Refer to Web version on PubMed Central for supplementary material.

Acknowledgements

This work was funded by the Arnall Patz Distinguished Professorship endowment (to R.M.K.), NEI grant number R01 EY025304 (to R.M.K.), and NINDS grant number R01NS093416 (to S.K.). We kindly thank the Wilmer Core Grant for Vision, Research, Microscopy, and Imaging Core Module (Grant #EY001865) for access to the Leica CM 1905 cryostat and Zen LSM710 confocal microscope.

References

[1]. Ung N, Yang I, Nanotechnology to augment immunotherapy for the treatment of glioblastoma multiforme, Journal of Neuro-Oncology, 123 (2015) 473–481. [PubMed: 26070553]

[2]. Adamson CD, Kanu OO, Mehta AI, Di C, Lin N, Mattox AK, Bigner DD, Glioblastoma multiforme: a review of where we have been and where we are going, Expert Opinion on Investigational Drugs, 18 (2009) 1061–1083. [PubMed: 19555299]

[3]. Omuro A, DeAngelis LM, Glioblastoma and other malignant gliomas: A clinical review, JAMA, 310 (2013) 1842–1850. [PubMed: 24193082]

[4]. Wen PY, Kesari S, Malignant gliomas in adults, The New England journal of medicine, 359 (2008) 492–507. [PubMed: 18669428]

[5]. Asher A, Fu JB, Bailey C, Hughes JK, Fatigue among patients with brain tumors, CNS Oncol, 5 (2016) 91–100. [PubMed: 26987038]

[6]. Becker KP, Yu J, Status Quo—Standard-of-Care Medical and Radiation Therapy for Glioblastoma, The Cancer Journal, 18 (2012) 12–19. [PubMed: 22290252]

[7]. Dai Q, Wilhelm S, Ding D, Syed AM, Sindhwani S, Zhang Y, Chen YY, MacMillan P, Chan WCW, Quantifying the Ligand-Coated Nanoparticle Delivery to Cancer Cells in Solid Tumors, ACS Nano, 12 (2018) 8423–8435. [PubMed: 30016073]

[8]. Solinas G, Germano G, Mantovani A, Allavena P, Tumor-associated macrophages (TAM) as major players of the cancer-related inflammation, Journal of Leukocyte Biology, 86 (2009) 1065–1073. [PubMed: 19741157]

[9]. Sica A, Schioppa T, Mantovani A, Allavena P, Tumour-associated macrophages are a distinct M2 polarised population promoting tumour progression: Potential targets of anti-cancer therapy, European Journal of Cancer, 42 (2006) 717–727. [PubMed: 16520032]

[10]. Lin EY, Nguyen AV, Russell RG, Pollard JW, Colony-Stimulating Factor 1 Promotes Progression of Mammary Tumors to Malignancy, Journal of Experimental Medicine, 193 (2001) 727–740.

[11]. Jeong H, Kim S, Hong B-J, Lee C-J, Kim Y-E, Bok S, Oh J-M, Gwak S-H, Yoo MY, Lee MS, Chung S-J, Defrêne J, Tessier P, Pelletier M, Jeon H, Roh T-Y, Kim B, Kim KH, Ju JH, Kim S, Lee Y-J, Kim D-W, Kim IH, Kim HJ, Park J-W, Lee Y-S, Lee JS, Cheon GJ, Weissman IL, Chung DH, Jeon YK, Ahn GO, Tumor-Associated Macrophages Enhance Tumor Hypoxia and Aerobic Glycolysis, Cancer Research, 79 (2019) 795. [PubMed: 30610087]

[12]. Lin Y, Xu J, Lan H, Tumor-associated macrophages in tumor metastasis: biological roles and clinical therapeutic applications, Journal of Hematology & Oncology, 12 (2019) 76. [PubMed: 31300030]

[13]. Sauter KA, Pridans C, Sehgal A, Tsai YT, Bradford BM, Raza S, Moffat L, Gow DJ, Beard PM, Mabbott NA, Smith LB, Hume DA, Pleiotropic effects of extended blockade of CSF1R signaling in adult mice, J Leukoc Biol, 96 (2014) 265–274. [PubMed: 24652541]

[14]. Radi ZA, Koza-Taylor PH, Bell RR, Obert LA, Runnels HA, Beebe JS, Lawton MP, Sadis S, Increased serum enzyme levels associated with kupffer cell reduction with no signs of hepatic or skeletal muscle injury, The American journal of pathology, 179 (2011) 240–247. [PubMed: 21703406]

[15]. Sun T, Zhang YS, Pang B, Hyun DC, Yang M, Xia Y, Engineered nanoparticles for drug delivery in cancer therapy, Angewandte Chemie (International ed. in English), 53 (2014) 12320–12364. [PubMed: 25294565]

[16]. Cieslewicz M, Tang J, Yu JL, Cao H, Zavaljevski M, Motoyama K, Lieber A, Raines EW, Pun SH, Targeted delivery of proapoptotic peptides to tumor-associated macrophages improves survival, Proceedings of the National Academy of Sciences, 110 (2013) 15919.

[17]. Conde J, Bao C, Tan Y, Cui D, Edelman ER, Azevedo HS, Byrne HJ, Artzi N, Tian F, Dual Targeted Immunotherapy via In Vivo Delivery of Biohybrid RNAi-Peptide Nanoparticles to Tumor-Associated Macrophages and Cancer Cells, Advanced Functional Materials, 25 (2015) 4183–4194. [PubMed: 27340392]

[18]. Azad AK, Rajaram MVS, Schlesinger LS, Exploitation of the Macrophage Mannose Receptor (CD206) in Infectious Disease Diagnostics and Therapeutics, J Cytol Mol Biol, 1 (2014) 1000003. [PubMed: 24672807]

[19]. Calvaresi EC, Hergenrother PJ, Glucose conjugation for the specific targeting and treatment of cancer, Chemical science, 4 (2013) 2319–2333. [PubMed: 24077675]

[20]. Sztandera K, Działak P, Marcinkowska M, Stańczyk M, Gorzkiewicz M, Janaszewska A, Klajnert-Maculewicz B, Sugar Modification Enhances Cytotoxic Activity of PAMAM-Doxorubicin Conjugate in Glucose-Deprived MCF-7 Cells – Possible Role of GLUT1 Transporter, Pharmaceutical Research, 36 (2019) 140. [PubMed: 31367876]

[21]. Zhao P, Wang Y, Kang X, Wu A, Yin W, Tang Y, Wang J, Zhang M, Duan Y, Huang Y, Dual-targeting biomimetic delivery for anti-glioma activity via remodeling the tumor microenvironment and directing macrophage-mediated immunotherapy, Chemical science, 9 (2018) 2674–2689. [PubMed: 29732051]

[22]. Zhao M, van Straten D, Broekman MLD, Préat V, Schiffelers RM, Nanocarrier-based drug combination therapy for glioblastoma, Theranostics, 10 (2020) 1355–1372. [PubMed: 31938069]

[23]. Lesniak WG, Mishra MK, Jyoti A, Balakrishnan B, Zhang F, Nance E, Romero R, Kannan S, Kannan RM, Biodistribution of fluorescently labeled PAMAM dendrimers in neonatal rabbits: effect of neuroinflammation, Molecular pharmaceutics, 10 (2013) 4560–4571. [PubMed: 24116950]

[24]. Zhang F, Mastorakos P, Mishra MK, Mangraviti A, Hwang L, Zhou J, Uniform brain tumor distribution and tumor associated macrophage targeting of systemically administered dendrimers, Biomaterials, 52 (2015).

[25]. Srinageshwar B, Peruzzaro S, Andrews M, Johnson K, Hietpas A, Clark B, McGuire C, Petersen E, Kippe J, Stewart A, Lossia O, Al-Gharaibeh A, Antcliff A, Culver R, Swanson D, Dunbar G, Sharma A, Rossignol J, PAMAM Dendrimers Cross the Blood–Brain Barrier When Administered through the Carotid Artery in C57BL/6J Mice, International Journal of Molecular Sciences, 18 (2017) 628.

[26]. Sharma A, Sharma R, Zhang Z, Liaw K, Kambhampati SP, Porterfield JE, Lin KC, DeRidder LB, Kannan S, Kannan RM, Dense hydroxyl polyethylene glycol dendrimer targets activated glia in multiple CNS disorders, Science Advances, 6 (2020) eaay8514. [PubMed: 32010790]

[27]. Sharma R, Kambhampati SP, Zhang Z, Sharma A, Chen S, Duh EI, Kannan S, Tso MOM, Kannan RM, Dendrimer mediated targeted delivery of sinomenine for the treatment of acute neuroinflammation in traumatic brain injury, Journal of Controlled Release, 323 (2020) 361–375. [PubMed: 32339548]

[28]. Sharma R, Sharma A, Kambhampati SP, Reddy RR, Zhang Z, Cleland JL, Kannan S, Kannan RM, Scalable synthesis and validation of PAMAM dendrimer-N-acetyl cysteine conjugate for potential translation, Bioengineering & translational medicine, 3 (2018) 87–101. [PubMed: 30065965]

[29]. Nemeth CL, Tomlinson SN, Sharma R, Sharma A, Kannan S, Kannan RM, Fatemi A, Glial restricted precursor delivery of dendrimer N-acetylcysteine promotes migration and differentiation following transplant in mouse white matter injury model, Nanoscale, 12 (2020) 16063–16068. [PubMed: 32724988]

[30]. Mignani S, Majoral J-P, Dendrimers as macromolecular tools to tackle from colon to brain tumor types: a concise overview, New Journal of Chemistry, 37 (2013) 3337–3357.

[31]. Ban J, Li S, Zhan Q, Li X, Xing H, Chen N, Long L, Hou X, Zhao J, Yuan X, PMPC Modified PAMAM Dendrimer Enhances Brain Tumor-Targeted Drug Delivery, Macromolecular Bioscience, n/a 2000392.

[32]. Liu C, Zhao Z, Gao H, Rostami I, You Q, Jia X, Wang C, Zhu L, Yang Y, Enhanced blood-brain-barrier penetrability and tumor-targeting efficiency by peptide-functionalized poly(amidoamine) dendrimer for the therapy of gliomas, Nanotheranostics, 3 (2019) 311–330. [PubMed: 31687320]

[33]. Nance E, Kambhampati SP, Smith ES, Zhang Z, Zhang F, Singh S, Johnston MV, Kannan RM, Blue ME, Kannan S, Dendrimer-mediated delivery of N-acetyl cysteine to microglia in a mouse model of Rett syndrome, Journal of Neuroinflammation, 14 (2017) 252. [PubMed: 29258545]

[34]. Sharma A, Porterfield JE, Smith E, Sharma R, Kannan S, Kannan RM, Effect of mannose targeting of hydroxyl PAMAM dendrimers on cellular and organ biodistribution in a neonatal brain injury model, Journal of Controlled Release, 283 (2018) 175–189. [PubMed: 29883694]

[35]. Zhang F, Trent Magruder J, Lin YA, Crawford TC, Grimm JC, Sciortino CM, Wilson MA, Blue ME, Kannan S, Johnston MV, Baumgartner WA, Kannan RM, Generation-6 hydroxyl PAMAM dendrimers improve CNS penetration from intravenous administration in a large animal brain injury model, Journal of controlled release : official journal of the Controlled Release Society, 249 (2017) 173–182. [PubMed: 28137632]

[36]. Sharma A, Liaw K, Sharma R, Thomas AG, Slusher BS, Kannan S, Kannan RM, Targeting Mitochondria in Tumor-Associated Macrophages using a Dendrimer-Conjugated TSPO Ligand that Stimulates Antitumor Signaling in Glioblastoma, Biomacromolecules, 21 (2020) 3909–3922. [PubMed: 32786523]

[37]. Sharma A, Liaw K, Sharma R, Zhang Z, Kannan S, Kannan RM, Targeting Mitochondrial Dysfunction and Oxidative Stress in Activated Microglia using Dendrimer-Based Therapeutics, Theranostics, 8 (2018) 5529–5547. [PubMed: 30555562]

[38]. Sharma R, Kim S-Y, Sharma A, Zhang Z, Kambhampati SP, Kannan S, Kannan RM, Activated Microglia Targeting Dendrimer-Minocycline Conjugate as Therapeutics for Neuroinflammation, Bioconjugate Chemistry, 28 (2017) 2874–2886. [PubMed: 29028353]

[39]. Khoury ES, Sharma A, Ramireddy RR, Thomas AG, Alt J, Fowler A, Rais R, Tsukamoto T, Blue ME, Slusher B, Kannan S, Kannan RM, Dendrimer-conjugated glutaminase inhibitor selectively targets microglial glutaminase in a mouse model of Rett syndrome, Theranostics, 10 (2020) 5736–5748. [PubMed: 32483415]

[40]. Adekola K, Rosen ST, Shanmugam M, Glucose transporters in cancer metabolism, Curr Opin Oncol, 24 (2012) 650–654. [PubMed: 22913968]

[41]. Garber K, Energy Boost: The Warburg Effect Returns in a New Theory of Cancer, JNCI: Journal of the National Cancer Institute, 96 (2004) 1805–1806. [PubMed: 15601632]

[42]. Sharma R, Kottari N, Chabre YM, Abbassi L, Shiao TC, Roy R, A highly versatile convergent/divergent “onion peel” synthetic strategy toward potent multivalent glycodendrimers, Chemical Communications, 50 (2014) 13300–13303. [PubMed: 25227948]

[43]. Roy R, Shiao TC, Glyconanosynthons as powerful scaffolds and building blocks for the rapid construction of multifaceted, dense and chiral dendrimers, Chemical Society Reviews, 44 (2015) 3924–3941. [PubMed: 25556902]

[44]. Zhang Y, Chan JW, Moretti A, Uhrich KE, Designing polymers with sugar-based advantages for bioactive delivery applications, Journal of controlled release : official journal of the Controlled Release Society, 219 (2015) 355–368. [PubMed: 26423239]

[45]. Sharma A, Khatchadourian A, Khanna K, Sharma R, Kakkar A, Maysinger D, Multivalent niacin nanoconjugates for delivery to cytoplasmic lipid droplets, Biomaterials, 32 (2011) 1419–1429. [PubMed: 21071082]

[46]. Sharma R, Naresh K, Chabre YM, Rej R, Saadeh NK, Roy R, “Onion peel” dendrimers: a straightforward synthetic approach towards highly diversified architectures, Polymer Chemistry, 5 (2014) 4321–4331.

[47]. Sharma A, Liaw K, Sharma R, Spriggs T, Appiani La Rosa S, Kannan S, Kannan RM, Dendrimer-Mediated Targeted Delivery of Rapamycin to Tumor-Associated Macrophages Improves Systemic Treatment of Glioblastoma, Biomacromolecules, 21 (2020) 5148–5161. [PubMed: 33112134]

[48]. Zhu S, Niu M, O'Mary H, Cui Z, Targeting of Tumor-Associated Macrophages Made Possible by PEG-Sheddable, Mannose-Modified Nanoparticles, Molecular pharmaceutics, 10 (2013) 3525–3530. [PubMed: 23901887]

[49]. Tekade RK, Sun X, The Warburg effect and glucose-derived cancer theranostics, Drug Discovery Today, 22 (2017) 1637–1653. [PubMed: 28843632]

[50]. Lai IL, Chou C-C, Lai P-T, Fang C-S, Shirley LA, Yan R, Mo X, Bloomston M, Kulp SK, Bekaii-Saab T, Chen C-S, Targeting the Warburg effect with a novel glucose transporter inhibitor to overcome gemcitabine resistance in pancreatic cancer cells, Carcinogenesis, 35 (2014) 2203–2213. [PubMed: 24879635]

[51]. el Khoury J, Thomas CA, Loike JD, Hickman SE, Cao L, Silverstein SC, Macrophages adhere to glucose-modified basement membrane collagen IV via their scavenger receptors, The Journal of biological chemistry, 269 (1994) 10197–10200. [PubMed: 8144597]

[52]. Thijssen VLJL, Poirier F, Baum LG, Griffioen AW, Galectins in the tumor endothelium: opportunities for combined cancer therapy, Blood, 110 (2007) 2819–2827. [PubMed: 17591944]

[53]. Hittelet A, Legendre H, Nagy N, Bronckart Y, Pector J-C, Salmon I, Yeaton P, Gabius H-J, Kiss R, Camby I, Upregulation of galectins-1 and −3 in human colon cancer and their role in regulating cell migration, International Journal of Cancer, 103 (2003) 370–379. [PubMed: 12471620]

[54]. Longmire M, Choyke PL, Kobayashi H, Clearance properties of nano-sized particles and molecules as imaging agents: considerations and caveats, Nanomedicine (Lond), 3 (2008) 703–717. [PubMed: 18817471]

[55]. Griffith LG, Lopina S, Microdistribution of substratum-bound ligands affects cell function: hepatocyte spreading on PEO-tethered galactose, Biomaterials, 19 (1998) 979–986. [PubMed: 9692796]

[56]. Duan C, Gao J, Zhang D, Jia L, Liu Y, Zheng D, Liu G, Tian X, Wang F, Zhang Q, Galactose-Decorated pH-Responsive Nanogels for Hepatoma-Targeted Delivery of Oridonin, Biomacromolecules, 12(2011)4335–4343. [PubMed: 22077387]

[57]. Lanthier N, Targeting Kupffer cells in non-alcoholic fatty liver disease/non-alcoholic steatohepatitis: Why and how?, World J Hepatol, 7 (2015) 2184–2188. [PubMed: 26380042]

[58]. Ganesan LP, Mohanty S, Kim J, Clark KR, Robinson JM, Anderson CL, Rapid and efficient clearance of blood-borne virus by liver sinusoidal endothelium, PLoS Pathog, 7 (2011) e1002281–e1002281. [PubMed: 21980295]

[59]. Magnusson S, Berg T, Extremely rapid endocytosis mediated by the mannose receptor of sinusoidal endothelial rat liver cells, Biochemical Journal, 257 (1989) 651–656.

[60]. Murray GJ, Jin FS, Immunoelectron microscopic localization of mannose-terminal glucocerebrosidase in lysosomes of rat liver Kupffer cells, The journal of histochemistry and cytochemistry : official journal of the Histochemistry Society, 43 (1995) 149–158. [PubMed: 7822772]

[61]. Serwer LP, Noble CO, Michaud K, Drummond DC, Kirpotin DB, Ozawa T, Prados MD, Park JW, James CD, Investigation of intravenous delivery of nanoliposomal topotecan for activity against orthotopic glioblastoma xenografts, Neuro-Oncology, 13 (2011) 1288–1295. [PubMed: 21954443]

[62]. Peng C, Gao X, Xu J, Du B, Ning X, Tang S, Bachoo RM, Yu M, Ge WP, Zheng J, Targeting orthotopic gliomas with renal-clearable luminescent gold nanoparticles, Nano research, 10 (2017) 1366–1376. [PubMed: 29034063]

[63]. Zou Y, Liu Y, Yang Z, Zhang D, Lu Y, Zheng M, Xue X, Geng J, Chung R, Shi B, Effective and Targeted Human Orthotopic Glioblastoma Xenograft Therapy via a Multifunctional Biomimetic Nanomedicine, Advanced materials (Deerfield Beach, Fla.), 30 (2018) e1803717.

[64]. Ganipineni LP, Ucakar B, Joudiou N, Bianco J, Danhier P, Zhao M, Bastiancich C, Gallez B, Danhier F, Préat V, Magnetic targeting of paclitaxel-loaded poly(lactic-co-glycolic acid)-based nanoparticles for the treatment of glioblastoma, Int J Nanomedicine, 13 (2018) 4509–4521. [PubMed: 30127603]

[65]. Hu G, Zhang H, Zhang L, Ruan S, He Q, Gao H, Integrin-mediated active tumor targeting and tumor microenvironment response dendrimer-gelatin nanoparticles for drug delivery and tumor treatment, International Journal of Pharmaceutics, 496 (2015) 1057–1068. [PubMed: 26598487]

[66]. Thorens B, Glucose transporters in the regulation of intestinal, renal, and liver glucose fluxes, American Journal of Physiology - Gastrointestinal and Liver Physiology, 270 (1996) G541–G553.

[67]. Stockert RJ, Morell AG, Hepatic Binding Protein: The Galactose-Specific Receptor of Mammalian Hepatocytes, Hepatology, 3 (1983) 750–757. [PubMed: 6413351]

[68]. Prabhu S, Goda JS, Mutalik S, Mohanty BS, Chaudhari P, Rai S, Udupa N, Rao BSS, A polymeric temozolomide nanocomposite against orthotopic glioblastoma xenograft: tumor-specific homing directed by nestin, Nanoscale, 9 (2017) 10919–10932. [PubMed: 28731079]

[69]. Song J, Yang X, Jacobson O, Huang P, Sun X, Lin L, Yan X, Niu G, Ma Q, Chen X, Ultrasmall Gold Nanorod Vesicles with Enhanced Tumor Accumulation and Fast Excretion from the Body for Cancer Therapy, Advanced Materials, 27 (2015) 4910–4917. [PubMed: 26198622]

[70]. Kurata T, Oguri T, Isobe T, Ishioka S, Yamakido M, Differential expression of facilitative glucose transporter (GLUT) genes in primary lung cancers and their liver metastases, Japanese journal of cancer research : Gann, 90 (1999) 1238–1243. [PubMed: 10622535]

[71]. Lu H, Buchan RJ, Cook SA, MicroRNA-223 regulates Glut4 expression and cardiomyocyte glucose metabolism, Cardiovascular Research, 86 (2010) 410–420. [PubMed: 20080987]

[72]. Haworth JC, Ford JD, Younoszai MK, Effect of Galactose Toxicity on Growth of the Rat Fetus and Brain, Pediatric Research, 3 (1969) 441–447. [PubMed: 5343540]

[73]. Malide D, Davies-Hill TM, Levine M, Simpson IA, Distinct localization of GLUT-1, −3, and −5 in human monocyte-derived macrophages: effects of cell activation, American Journal of Physiology- Endocrinology and Metabolism, 274 (1998) E516–E526.

[74]. Freemerman AJ, Johnson AR, Sacks GN, Milner JJ, Kirk EL, Troester MA, Macintyre AN, Goraksha-Hicks P, Rathmell JC, Makowski L, Metabolic reprogramming of macrophages: glucose transporter 1 (GLUT1)-mediated glucose metabolism drives a proinflammatory phenotype, The Journal of biological chemistry, 289 (2014) 7884–7896. [PubMed: 24492615]

[75]. Wang H-W, Joyce JA, Alternative activation of tumor-associated macrophages by IL-4, Cell Cycle, 9 (2010) 4824–4835. [PubMed: 21150330]

[76]. Liaw K, Gök O, DeRidder LB, Kannan S, Kannan RM, Quantitative assessment of surface functionality effects on microglial uptake and retention of PAMAM dendrimers, Journal of Nanoparticle Research, 20 (2018) 111.

[77]. Farrell CL, Pardridge WM, Blood-brain barrier glucose transporter is asymmetrically distributed on brain capillary endothelial lumenal and ablumenal membranes: an electron microscopic immunogold study, Proceedings of the National Academy of Sciences, 88 (1991) 5779.

[78]. Camby I, Belot N, Rorive S, Lefranc F, Maurage C-A, Lahm H, Kaltner H, Hadari Y, Ruchoux M-M, Brotchi J, Zick E, Salmon I, Gabius H-J, Kiss R, Galectins Are Differentially Expressed in Supratentorial Pilocytic Astrocytomas, Astrocytomas, Anaplastic Astrocytomas and Glioblastomas, and Significantly Modulate Tumor Astrocyte Migration, Brain Pathology, 11 (2001) 12–26. [PubMed: 11145198]

[79]. Inufusa H, Nakamura M, Adachi T, Aga M, Kurimoto M, Nakatani Y, Wakano T, Miyake M, Okuno K, Shiozaki H, Yasutomi M, Role of galectin-3 in adenocarcinoma liver metastasis, International journal of oncology, 19 (2001) 913–919. [PubMed: 11604988]

- Systemic targeting of TAMs can provide promising immunotherapeutic options for GBM
- Hydroxyl PAMAM dendrimers target TAMs from systemic administration
- Glycosylation of PAMAM-OH significantly improves TAMs targeting and specificity
- These dendrimers are promising platform for enhanced anti-cancer drug delivery

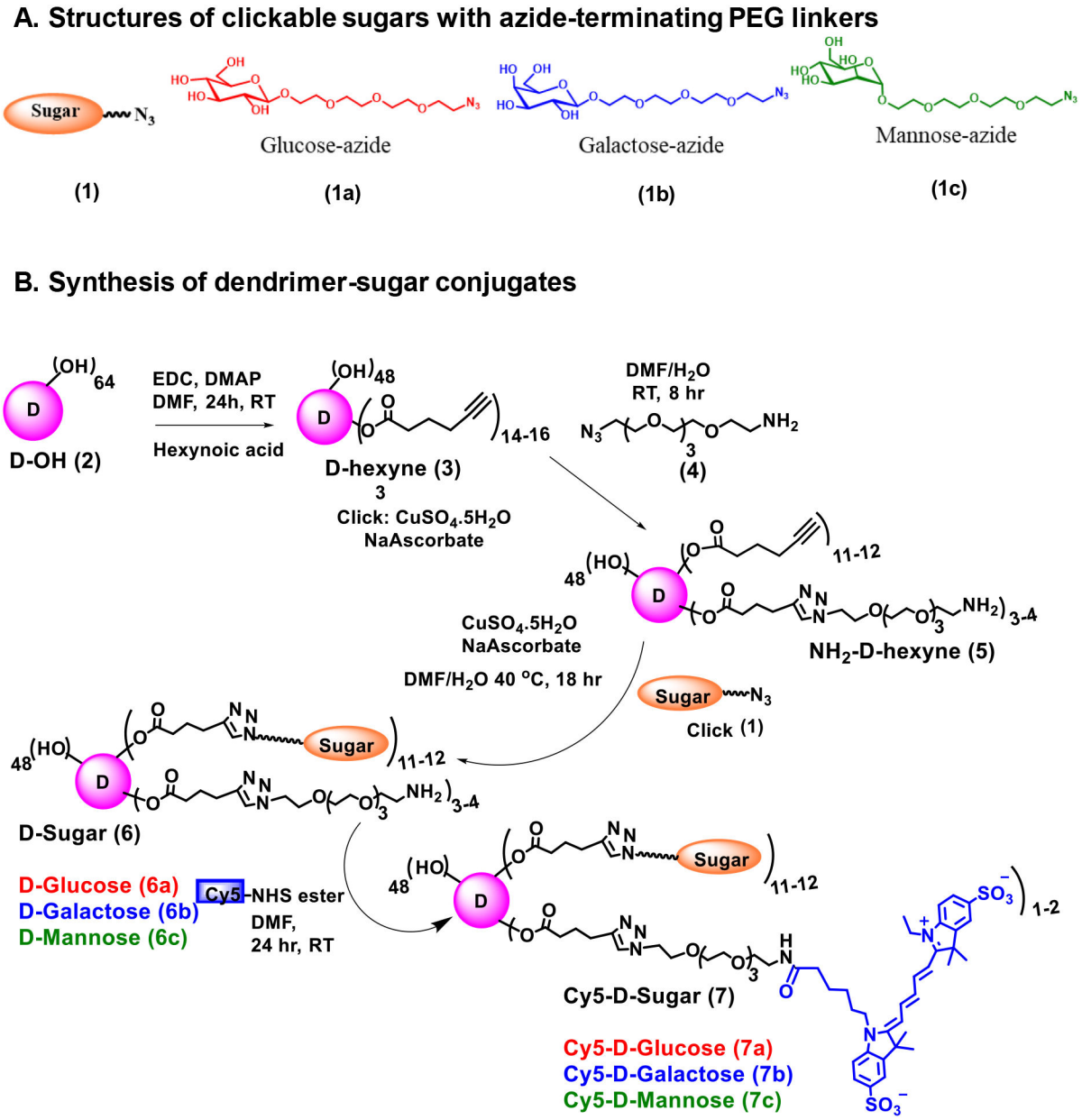

Figure 1.

A. Structural representation of clickable sugars. The structures of glucose-azide, galactose-azide and mannose-azide with PEG linkers (β-D-Glucose-PEG4-azide (1a), β-D-Galactose-PEG4-azide (1b), and α-D-Mannose-PEG4-azide (1c)) are presented; **B. Synthetic protocol for dendrimer-sugar conjugates.** The synthesis of fluorescently labeled **Cy5-D-Glucose, Cy5-D-Mannose**, and **Cy5-D-Galactose** is presented using CuAAC click chemistry approach.

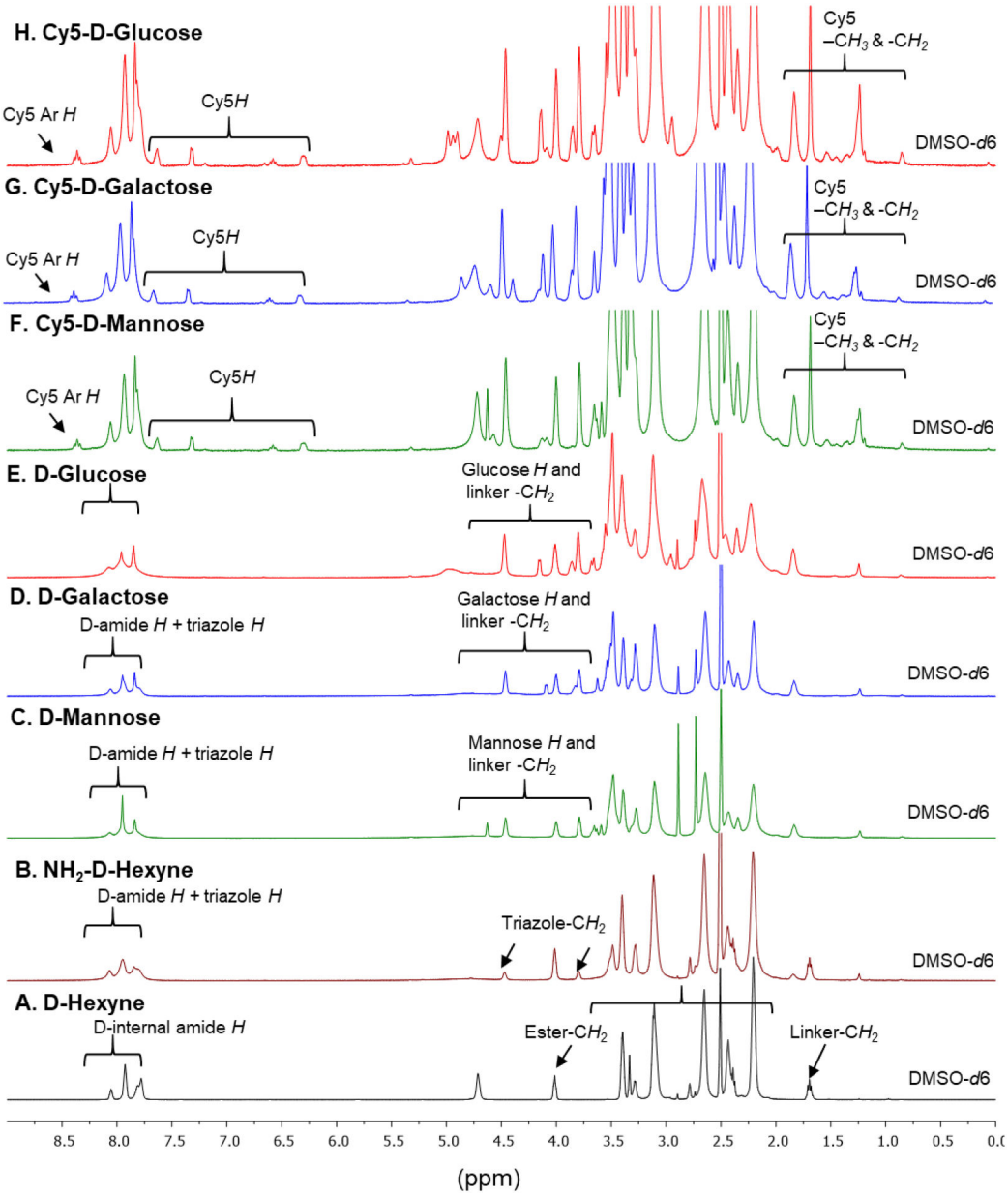

Figure 2A-H. ^{1}H NMR comparison of intermediates, D-Sugars and fluorescently labeled dendrimer conjugates.

The spectra show the appearance of characteristic signal corresponding to sugar protons and Cy5 protons along with the parent dendrimer protons. The integration comparison of sugar and Cy5 protons to internal amide protons from dendrimer was utilized to calculate the number of conjugated ligands.

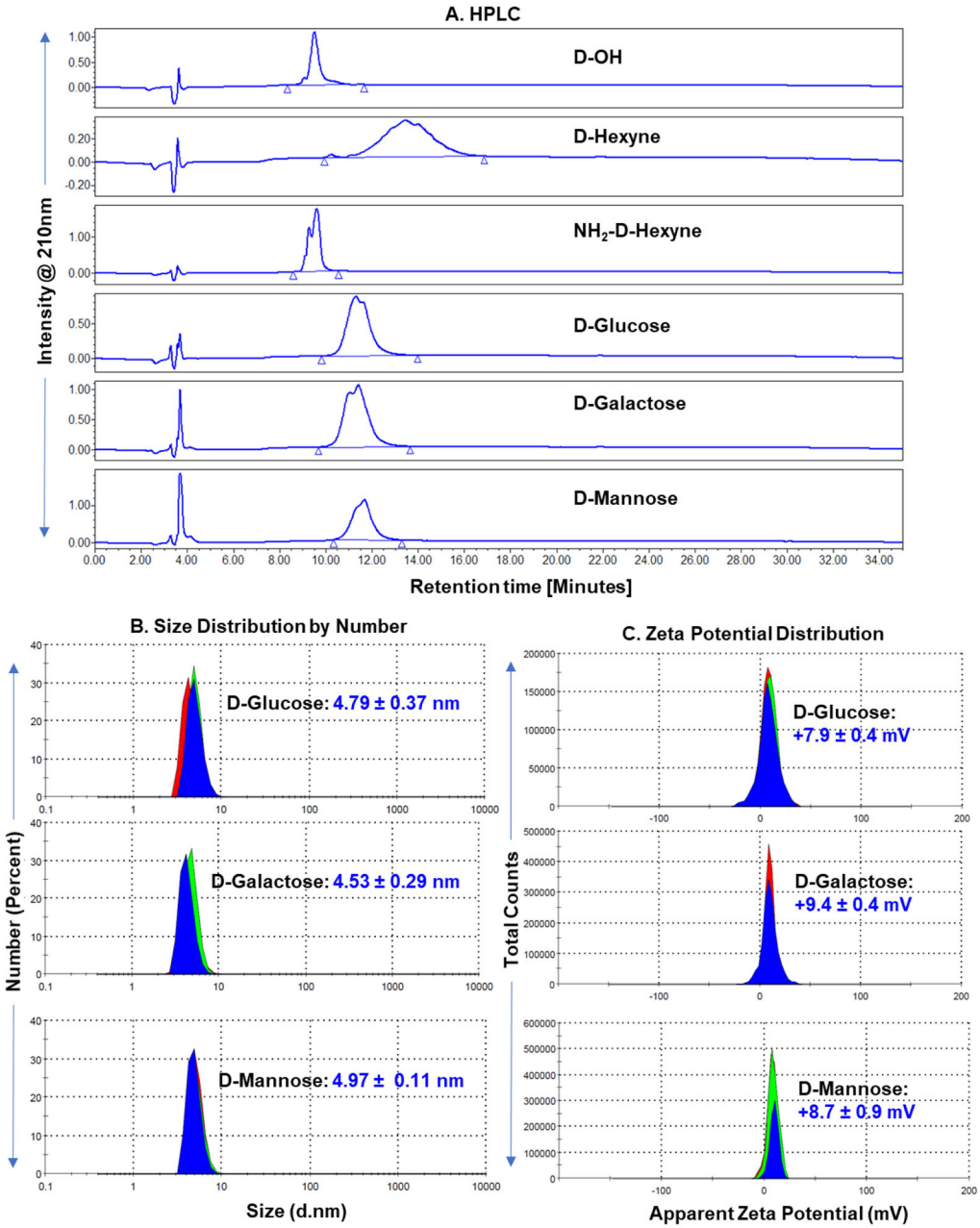

Figure 3. Physio-chemical characterization of dendrimer conjugates.

A. HPLC comparison of parent hydroxyl dendrimer (D-OH, RT: 9.5 min), alkyne-terminating dendrimer (D-Hexyne, RT: 13.4 min), trifunctional dendrimer (NH_2-D-Hexyne, RT: 9.6 min), and sugar modified dendrimers (**D-Glucose**, RT: 11.3 min; **D- Galactose**, RT: 11.4 min; and **D- Mannose**, RT: 11.7 min). All the intermediates and sugar conjugates have >99% purity. **B.** Hydrodynamic diameter measurements of **D-Sugars** via dynamic light scattering. The dendrimer conjugates show a slight increase in size from D-OH (~4 nm). **C.** Representation of zeta potential distribution measurements of **D-Sugars** showing nearly neutral zeta potential.

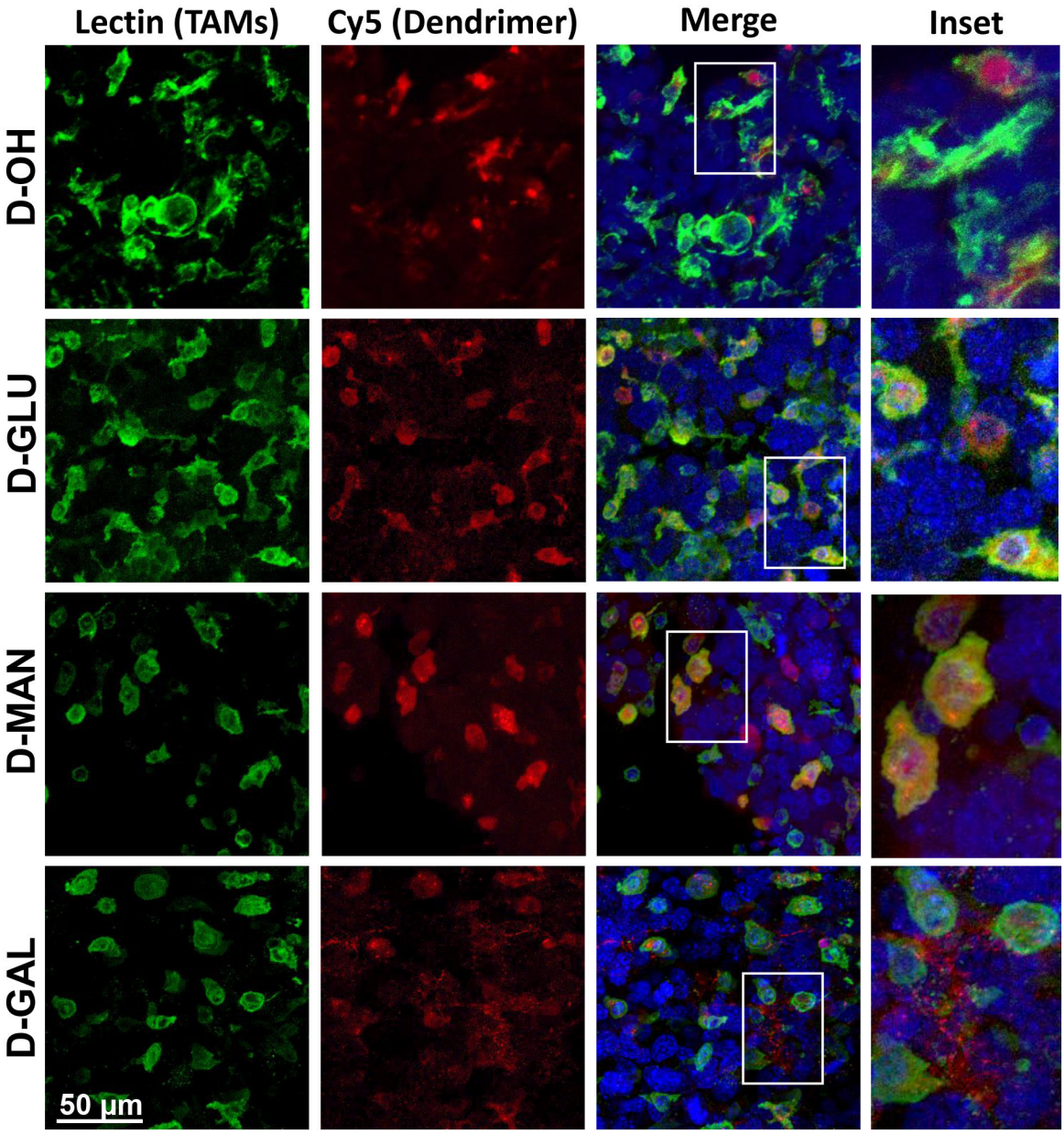

Figure 4. Sugar-conjugated dendrimer localization with tumor-associated macrophages and microglia in glioblastoma.

Glioblastoma brain tumor-bearing mice were injected with various dendrimers on day 14 after inoculation. Brains were collected 24 hours after administration, fixed, and stained with lectin to label tumor-associated macrophages/microglia (TAMs, green) and DAPI to label nuclei (blue) for confocal microscopy to visualize dendrimer (red) localization. Unmodified dendrimer (**D-OH**) localizes to TAMs within the tumor upon systemic administration. Glucose- (**D-GLU**) and mannose-conjugated dendrimers (**D-MAN**) maintain the TAMs localization of **D-OH**. Galactose-conjugated dendrimer (**D-GAL**) exhibits some TAMs localization, with additional signal observed in the extracellular space.

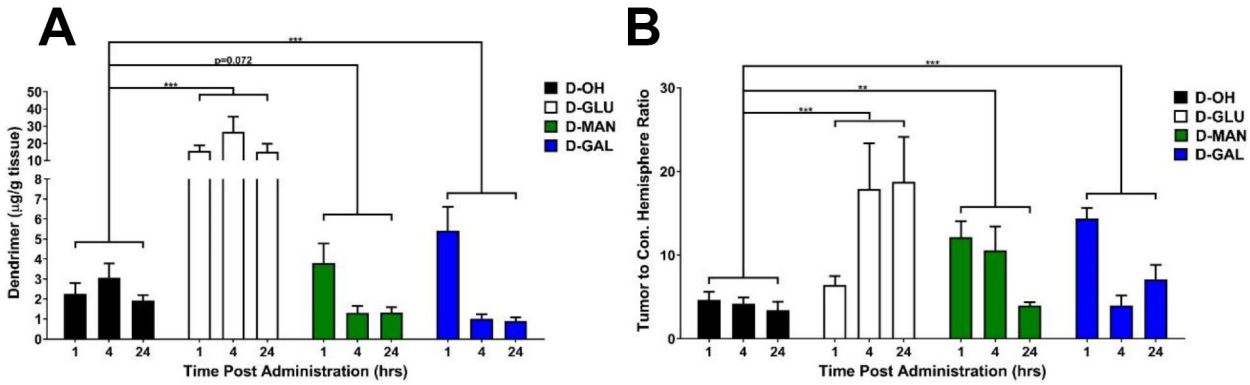

Figure 5. Sugar conjugation alters tumor accumulation kinetics of dendrimers and increases tumor specificity.

Glioblastoma brain tumor-bearing mice were injected intravenously with various dendrimers on day 14 after tumor inoculation. Brains were collected 24 hours after injection, homogenized, and dendrimer content was measured via fluorescence spectrometry. **A)** Brain tumor-bearing mice injected with glucose- (**D-GLU**), mannose (**D-MAN**), and galactose-conjugated dendrimers (**D-GAL**) exhibit significantly greater tumor accumulation than unmodified dendrimers (**D-OH**). *** $p < 0.001$. **B**) Sugar-conjugated dendrimers exhibit significantly greater specificity for the tumor compared to the contralateral hemisphere than unmodified dendrimers. ** $p < 0.01$, *** $p < 0.001$.

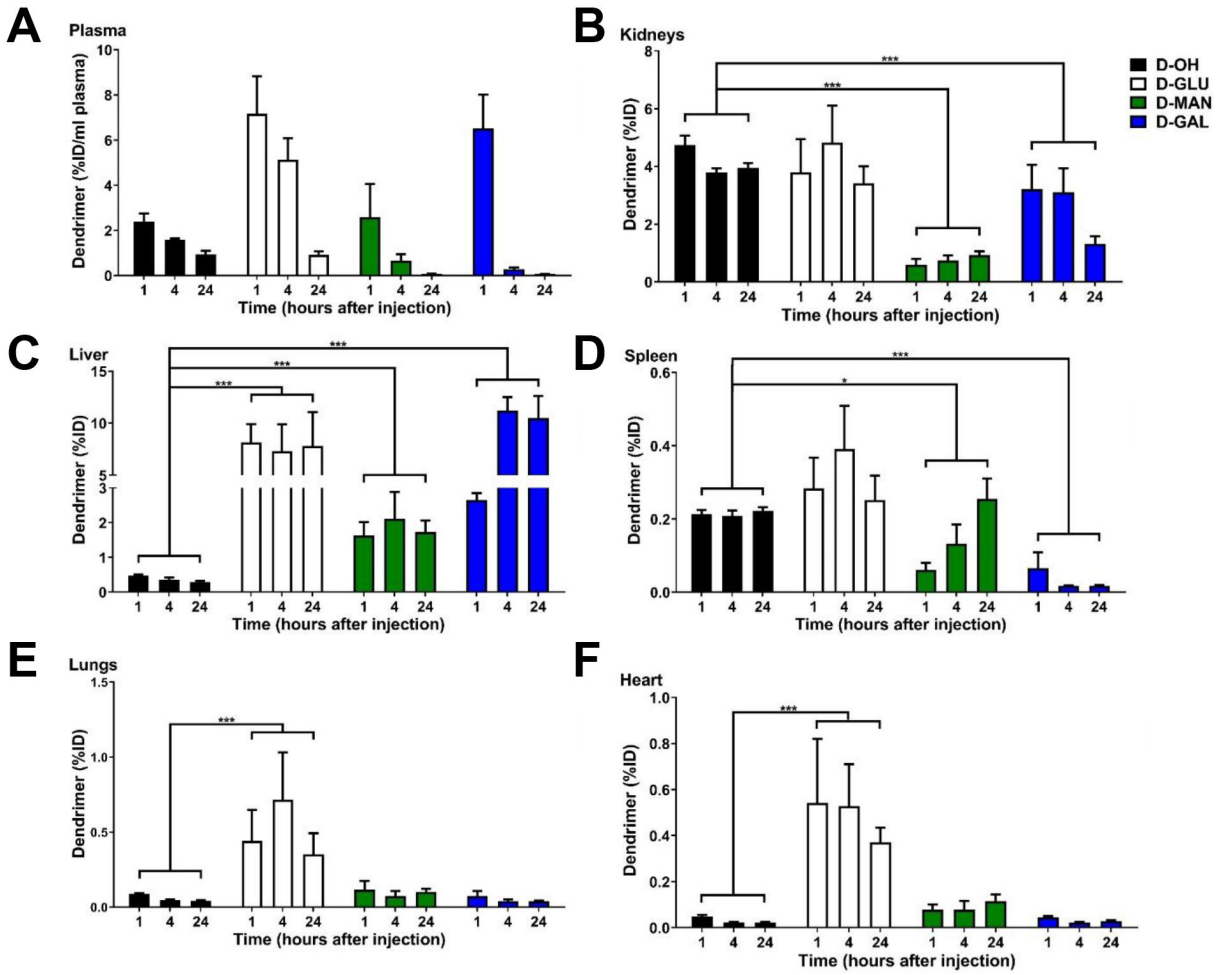

Figure 6. Systemic biodistribution of sugar-conjugated dendrimers compared to unmodified dendrimers.

Glioblastoma bearing mice were injected with unmodified (**D-OH**), glucose- (**D-GLU**), mannose- (**D-MAN**), and galactose-conjugated (**D-GAL**) dendrimers on day 14 after tumor inoculation. All dendrimers rapidly clear from the body, with less than 1% of the initial injected dose remaining per mL of plasma after 24 hours. Conjugation with sugars alters systemic biodistribution. * $p < 0.05$, ** $p < 0.01$, *** $p < 0.001$.

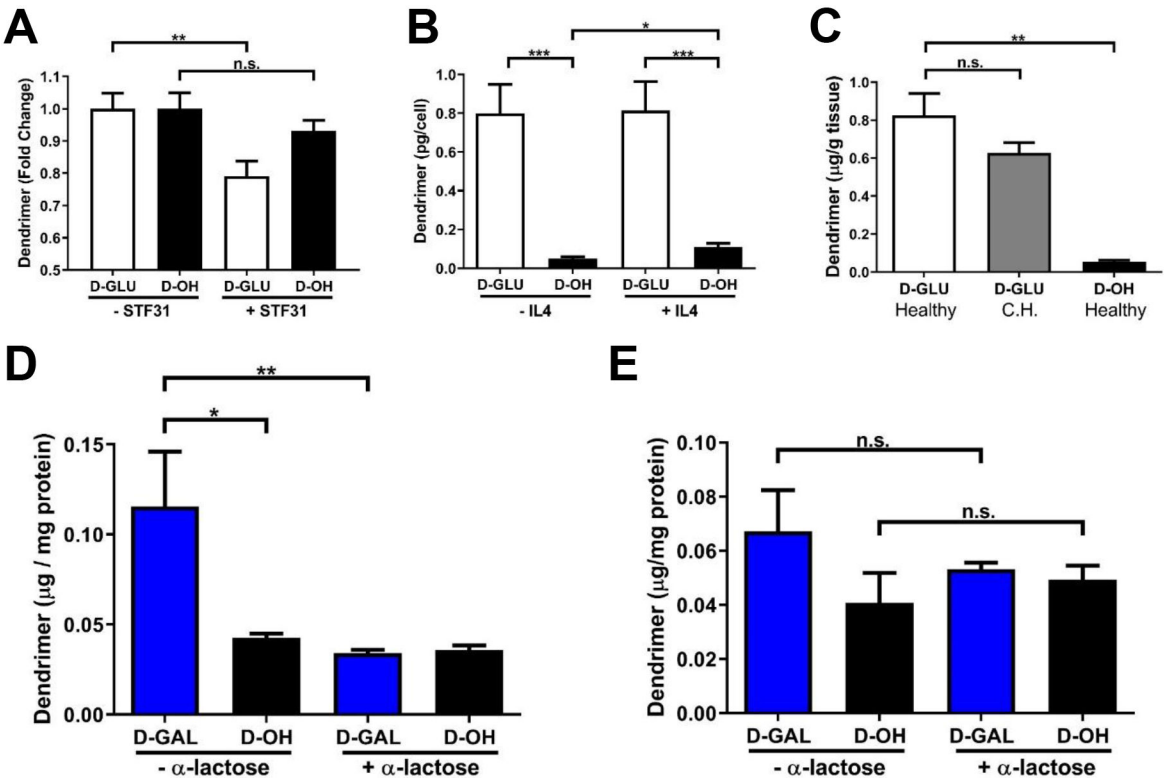

Figure 7. Dendrimer-glucose and -galactose conjugates alter cellular interactions.

A) Blocking GLUT-1 receptors on BV2 murine microglia by STF-31 reduces dendrimer-glucose (**D-GLU**) cellular internalization but does not impact uptake of unmodified dendrimers (**D-OH**), validating the GLUT-1 uptake mechanism of **D-GLU**. ** $p < 0.01$D, n.s. $p > 0.1$. **B)** Dendrimer internalization in IL4 and resting microglia is significantly greater with **D-GLU** than **D-OH**, indicating improved cellular internalization. * $p < 0.05$, *** $p < 0.001$. **C) D-GLU** exhibits similar brain uptake in healthy brain tissue and in the contralateral hemisphere of tumor-bearing brains and significantly greater than **D-OH**, indicating increased blood brain barrier penetration. ** $p < 0.01$, n.s. $p > 0.1$. **D)** Dendrimer-galactose conjugates (**D-GAL**) exhibits significantly greater membrane association in GL261 murine glioma cells than **D-OH**. Blocking of galectins with α-lactose knocks membrane levels of **D-GAL** down to similar levels as **D-OH**, validating D-GAL interactions with galectin surface receptors. * $p < 0.05$, ** $p < 0.01$. **E)** Cellular uptake of dendrimers of **D-GAL** is not altered with α-lactose treatment, indicating that **D-GAL** interactions with galectin receptors does not impact cellular internalization. n.s. $p > 0.1$.